

TRACE-ELEMENT DISTRIBUTION IN CASSITERITE AND SULFIDES FROM RUBANÉ AND MASSIVE ORES OF THE CORVO DEPOSIT, PORTUGAL

SILVIA SERRANTI[§]

*Dipartimento di Ingegneria Chimica, dei Materiali, delle Materie Prime e Metallurgia, Università di Roma "La Sapienza",
Via Eudossiana 18, I-00184 Roma, Italy*

VINCENZO FERRINI AND UMBERTO MASI

Dipartimento di Scienze della Terra, Università di Roma "La Sapienza", P.le Aldo Moro 5, I-00185 Roma, Italy

LOUIS J. CABRI

99 Fifth Avenue, Suite 122, Ottawa, Ontario K1S 5P5, Canada

ABSTRACT

A large number of samples containing sulfides, sulfosalts and cassiterite from the Corvo volcanogenic massive sulfide deposit, exploited at the Neves–Corvo mine, southern Portugal, were analyzed using electron and proton microprobes after a detailed examination by reflected-light ore microscopy. The samples are representative of the main four types of ore: cupriferous *rubané* ore, *rubané* ore with tin, cupriferous massive sulfide ore and cupriferous massive sulfide ore with tin. The trace-element distribution among the minerals from the four ores, and particularly the high Sn and In contents as well as the Se/S values of pyrite, provide evidence of a magmatic signature for this complex and unique deposit. With respect to cassiterite, which is a characteristic major ore mineral at the Corvo deposit, both chemical composition and textural relationships to sulfides suggest that the high-temperature reduced fluids that deposited sulfides also deposited cassiterite. The mineralogical and geochemical data support the field hypothesis of an allochthonous origin for *rubané* ores, inferred to be a part of the stockwork of massive mineralization, thrust on the top of massive ores during the Late Hercynian.

Keywords: Neves–Corvo, volcanogenic massive sulfide, Iberian Pyrite Belt, ore genesis, applied geochemistry, cassiterite, proton microprobe, Portugal.

SOMMAIRE

Nous avons analysé un grand nombre d'échantillons préalablement caractérisés par microscopie en lumière réfléchie, contenant sulfures, sulfosels et cassitérite, et provenant du gisement volcanogénique à sulfures massifs de Corvo, exploité à la mine Neves–Corvo, dans le sud du Portugal; nous nous sommes servis de microsondes électronique et protonique. Ces échantillons sont représentatifs de quatre types de minerai: minerai *rubané* cuprifère, minerai *rubané* stannifère, minerai cuprifère à sulfures massifs, et minerai cuprifère à sulfures massifs avec étain. La distribution des éléments traces parmi les minéraux des quatre types de minerai, et particulièrement la distribution de l'étain et de l'indium, à teneurs élevées, ainsi que les valeurs de Se/S dans la pyrite, semblent indiquer une origine magmatique de ce gisement complexe et unique. Pour ce qui est de la cassitérite, qui est une composante importante du minerai de ce gisement, la composition chimique et les relations texturales par rapport aux sulfures font penser que les fluides réducteurs de haute température à l'origine des sulfures l'ont aussi précipité. Les données minéralogiques et géochimiques étayent l'hypothèse formulée à partir des données de terrain à propos de l'origine allochthone des minerais *rubanés*, qui auraient fait partie de la zone nourricière située en-dessous de la minéralisation massive, et qui auraient par la suite été mis en place par chevauchement pendant l'orogénèse hercynienne tardive, pour maintenant se trouver au dessus des minerais massifs.

(Traduit par la Rédaction)

Mots-clés: Neves–Corvo, sulfures massifs volcanogéniques, Ceinture Pyriteuse Ibérique, genèse des minerais, géochimie appliquée, cassitérite, microsonde protonique, Portugal.

[§] E-mail address: silvia@imagemp.ing.uniroma1.it

INTRODUCTION

The Corvo orebody is one of five polymetallic lenses in the giant Neves–Corvo volcanogenic massive sulfide (VMS) deposit, discovered in 1977 in southern Portugal (Fig. 1). This deposit is one of 80 occurrences of sulfide mineralization found to date in the Iberian Pyrite Belt (IPB), which extends along an approximately E–W-trending arc about 230 km in length and 35 to 50 km in width. The Neves–Corvo deposit is currently the largest producer of Cu and Sn in Europe, with 1,091.8 Mt Cu and 26.3 Mt Sn produced from 1988 to 1997 (Real & Carvalho 1997).

A study of the compositional and textural attributes of the sulfides and cassiterite from the Corvo orebody was undertaken with the aim of defining the genesis of this mineralization and, thus, contributing to an understanding of the complex Neves–Corvo deposit (Serranti 1998). A study of the Corvo orebody is especially interesting because it exhibits two peculiar features: the highest tin contents known in VMS deposits and the presence of so-called *rubané* ore at the top of the main massive ore (Gaspar 1991). The term *rubané* was first used by BRGM geologists in the 1970s to indicate a ribbon-like occurrence of ore. Considering that the polymetallic ores are zoned laterally and vertically in major and trace elements (Pinto *et al.* 1997), we carried out a detailed analysis of trace-element distribution in minerals from the *rubané* and massive ores. In fact, the metallogenic implications of trace-element concentrations in sulfides and other minerals are well known and have increased

in importance since their first application following World War II (Fleischer 1955). The quality of trace-element data has improved over the years owing to application of increasingly more sensitive microbeam techniques.

In this paper, we report a large number of new chemical data for arsenopyrite, cassiterite, chalcopyrite, tetrahedrite–tennantite, k esterite, stannite, pyrite, sphalerite and chlorite from various types of ore in the Corvo orebody, and obtained by electron-probe microanalysis (EPMA) and micro-PIXE (proton-induced X-ray excitation).

GEOLOGICAL SETTING, MINERALIZATION AND TYPES OF ORE

The geology of the IPB has been the subject of several papers (*e.g.*, Carvalho *et al.* 1976, 1997, Strauss *et al.* 1977, Carvalho 1979, Routhier *et al.* 1980, Leistel *et al.* 1998). A small number of papers deals with the geology of the volcanogenic massive sulfide deposit of Neves–Corvo (*e.g.*, Albouy *et al.* 1981, Leca *et al.* 1983, Oliveira *et al.* 1997). This deposit is composed of five main orebodies, namely: Neves, Corvo, Graça, Zambujal and Lombador, characterized by higher copper and tin grades than other VMS deposits of the Iberian Pyrite Belt (Gaspar 1991, 1997, Oliveira *et al.* 1997). The main massive lenses lie above a stockwork located in the footwall felsic volcanosedimentary sequence of Early Tournaisian – Middle Viséan age. This sequence is concordant with phyllites and quartzites of

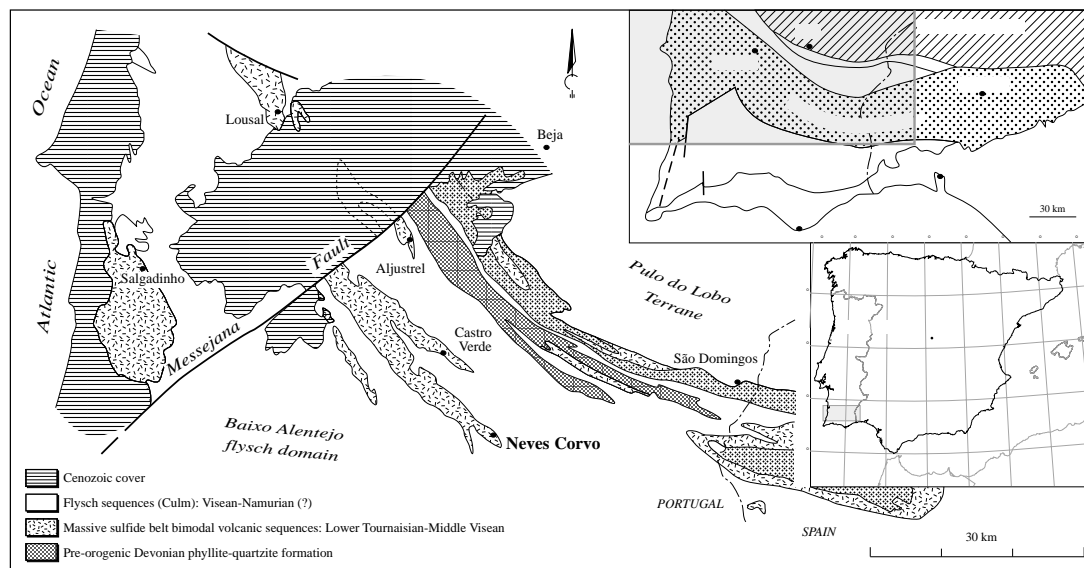


FIG. 1. Geological sketch-map of the Portuguese sector of the Iberian Pyrite Belt (IPB) and location of the Neves–Corvo VMS deposit. The inset maps show the location of the area depicted in the Iberian Peninsula (modified after Marcoux *et al.* 1996).

the Upper Devonian, and is covered by a Dinantian Culm-type flysch. All the rocks were folded and thrust during the Westphalian. The Neves–Corvo orebodies are distributed on both flanks of an open, asymmetrical anticline plunging to the southeast. In particular, the Corvo orebody (Fig. 2) is located on the northeastern flank of the anticline, with a NE–SW elongation, and dips 25° to 30° to the northeast, at depth of 230 to 1100 m along dip (Gaspar 2002).

The Neves–Corvo mineralization shows lateral and vertical zonation in metal distribution. Copper-rich sulfides usually occur at the base of the deposit and are in some cases overlain by zinc sulfides. “Barren” massive pyrite is generally located in the upper part of the orebody. Tin occurs in close spatial association with the Cu-enriched mineralization. Pyrite is the most abundant sulfide, followed by chalcopyrite, sphalerite and a host of other minerals. Cassiterite in places forms concentrations of economic importance. The mineral textures are complex because of fine intergrowths involving chalcopyrite, tetrahedrite–tennantite, sphalerite, pyrite and other minerals. Primary textures, such as colloform, soft-sediment flames and syngenetic folds, among oth-

ers, are preserved at some locations. Gangue minerals consist essentially of quartz, chlorite, white mica, dolomite and siderite.

At Neves–Corvo, three main types of ore are recognized (Oliveira *et al.* 1997): i) *rubané* ore, which occurs at the top of massive sulfides and is particularly well displayed in the Corvo orebody, ii) “massive sulfide”, which is the most abundant type of ore, and iii) “fissural” ores, occurring in the footwall rocks. Each type of ore has been further subdivided by SOMINCOR (Sociedade Mineira de Neves–Corvo) on the basis of the dominant mineral (Table 1). A detailed description of these types of ore is presented in Gaspar (1997, 2002).

Thinly banded shales, thin layers of sulfide, chert–carbonate breccias and massive sulfide lenses, which characterize *rubané* ore, are not present in the other deposits of the Iberian Pyrite Belt. Veinlets filled by chalcopyrite, pyrite and, in places, cassiterite commonly cross-cut the ore. *Rubané* ore is subdivided into a cassiterite-rich *rubané* ore (RT) and an overlying copper-rich *rubané* ore (RC). According to Relvas *et al.* (1997), Silva *et al.* (1997) and Cabri *et al.* (1998), the stratigraphic position of the *rubané* ore likely represents the

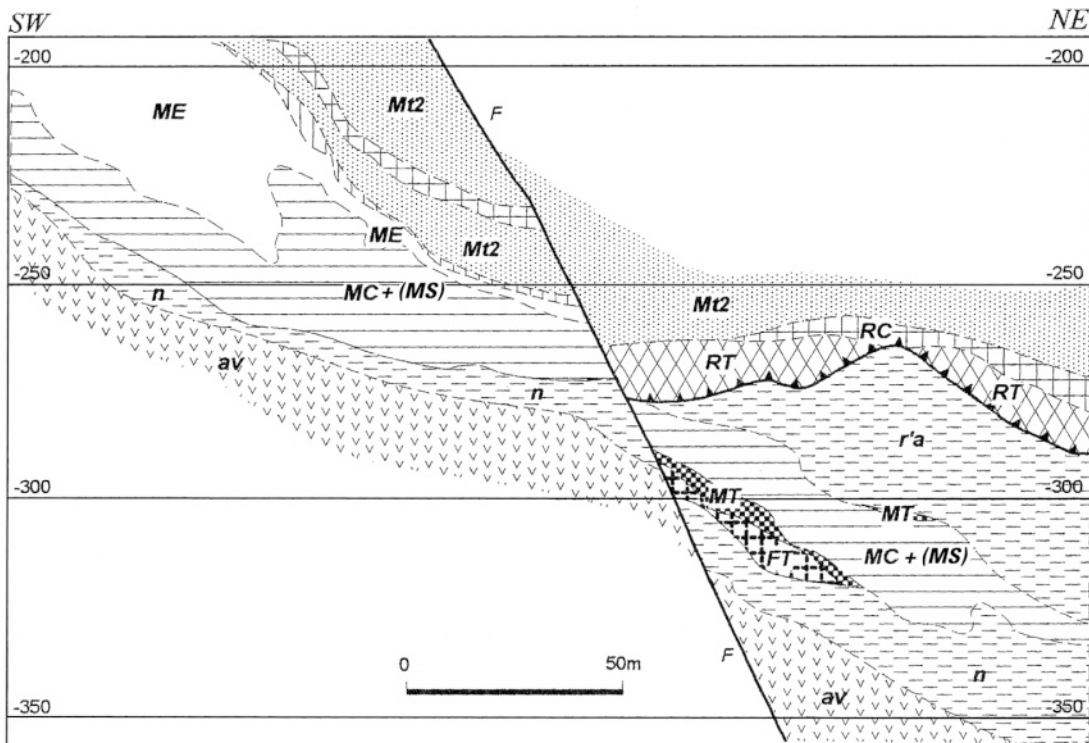


FIG. 2. Cross-section through the Corvo orebody (after SOMINCOR, unpubl. report). Lithological sequence: Mt2: greywakes and shales of the Mértola Formation; RC: cupriferous *rubané* ore; RT: *rubané* ore with tin; ME: massive pyritic ore; MC: cupriferous massive sulfide ore; r'a: black pyritic shale; MT: massive tin ore; FT: stockwork tin ore; n: black shales of the Neves Formation; av: felsic volcanic rocks.

result of thrusting, presumably owing to Late Hercynian tectonics, over massive ore, of which the *rubané* would represent part of the feeder zone. There is geological evidence in favor of such a hypothesis: i) the footwall contact of the *rubané* ore is a clear structural unconformity, transecting the stratigraphy; ii) there are unequivocal, multi-scale kinematic criteria in the internal structures; iii) the *rubané* ore lies partially on hanging-wall turbidites, which are about 20 Ma younger than the Corvo mineralization (Oliveira *et al.* 1997); iv) there is a clear lateral equivalence between the *rubané* ore and the uppermost footwall sequence (stockwork).

The massive ore is composed of fine-grained sulfides, mainly pyrite followed by chalcopyrite, sphalerite, tetrahedrite–tennantite, galena and other minerals. Cassiterite and minor stannite are the main tin-bearing minerals. Four main types of massive ore have been recognized (Table 1). MC is a massive cupriferous ore characterized by disseminations and bands of chalcopyrite within massive pyrite; MS is a massive type of ore richer in Cu than MC, and composed mainly of banded to massive chalcopyrite and containing cassiterite (Sn > 1%), whereas ME is a massive pyritic ore with low Cu, Zn and Sn contents, and MT is a locally developed massive cassiterite ore.

The “fissural” ore is the stockwork-type mineralization, occurring in the footwall shale and felsic volcanic rocks, usually as cross-cutting veinlets of sulfide minerals (pyrite and chalcopyrite with minor cassiterite and sphalerite). Two subtypes of fissural ore have been defined (Table 1).

SAMPLES AND ANALYTICAL METHODOLOGY

Thirty-five samples of bulk ore were collected from the *rubané* and massive ores of the Corvo orebody. The samples are representative of the four types of ore: i) cupriferous *rubané* ore (RC) from Level 752, ii) *rubané* ore with tin (RT) from Level 720, iii) cupriferous massive sulfide ore with tin (MS) from Level 717/3T, and iv) cupriferous massive sulfide ore (MC) from Level 740.

TABLE 1. CODES DESIGNATING ORE TYPES AT THE CORVO DEPOSIT, AS DEFINED ACCORDING TO THE TERMINOLOGY ADOPTED BY SOMINCOR*

Code	Description of ore type	Cut-off grades
RC	Cupriferous <i>rubané</i> ore	Cu > 2%
RT	<i>Rubané</i> ore with tin	Sn > 1%
ME	Massive pyritic ore	Zn < 1%, Cu < 2%, Sn < 1%
MC	Cupriferous massive sulfide ore	Cu > 2%
MS	Cupriferous massive ore with tin	Cu > 2%, Sn > 1%
MT	Massive tin ore	Sn > 8%
FC	Cupriferous fissural ore	Cu > 2%
FT	Fissural ore with tin	Sn > 1%

* Sociedade Mineira de Neves-Corvo.

The samples were prepared as polished thin sections for study by reflected and transmitted light microscopy. Some samples were cut into mm-sized cubes and reconstituted as polished sections for micro-PIXE analyses on selected areas of specific mineral grains.

The EPMA analyses were carried out at the Dipartimento di Scienze della Terra of the University of Rome “La Sapienza”, Italy, using a Cameca SX50 electron microprobe, and in the Mining and Mineral Sciences Laboratory of CANMET at Ottawa, Canada, using a JEOL–8900 electron microprobe. Both microprobes operated at 20 kV, beam current of 20 nA, counting for 20 s on major elements and 60 s for trace elements.

The micro-PIXE analyses were carried out at the Scanning Proton Microprobe Laboratory, Guelph–Waterloo Department of Physics Institute (University of Guelph), Guelph, Ontario, Canada, using a proton energy of 3 MeV with a beam size of approximately $7 \times 15 \mu\text{m}$ for a collected charge of 2.50 μC for each analysis. The current varied from 1.9 to 9.2 nA according to the mineral analyzed for analytical times varying from 1,285 to 273 s. A 125 μm Mylar film was used for attenuation of peaks due to major elements, as well as four different thicknesses of pure Al: 106, 247, 352 and 508 μm for cassiterite, pyrite, chalcopyrite, and tetrahedrite–tennantite, respectively. The spectra were processed using the 1996–08–30 version of the GUPIX software package (Maxwell *et al.* 1989, 1995). Simultaneous analyses were obtained with the proton microprobe for elements ranging in atomic number from ^{26}Fe to ^{83}Bi , with detection levels (MDL) of a few ppm, usually from 5 to 50, in the following minerals: chalcopyrite (13 grains), pyrite (16 grains), cassiterite (11 grains), tetrahedrite–tennantite (six grains) and stannite (four grains).

The Micro-PIXE technique is a non-destructive microbeam technique that is very similar to EPMA, as discussed by Remond *et al.* (1987). Some important differences between the two analytical methods were outlined by Cabri & Campbell (1998, p. 182). One of these differences is that the penetration depth of protons is much deeper than that of electrons, and the depth of penetration also depends on the elements and the density of the matrix. For example, with the Guelph configuration, calculated 90% X-ray yields at 3 MeV gives penetration depths for Se and Ag in chalcopyrite of 18.2 μm and 22.5 μm , respectively, in contrast to 13.7 μm and 14.8 μm in galena, respectively. Thus, not only is the volume sampled by PIXE much greater than by EPMA, but care must be taken to examine the results of trace-element analyses for the possibility of stray X-rays from subsurface inclusions, as discussed by Cabri & Campbell (1998, p. 186–189). Careful siting of the proton beam, together with interpretation of the anomalous results of analyses, are essential for meaningful results. The interpretation is simpler where there are few variables. In the case of the Neves–Corvo ores, however, the complexity of the mineralogy increases the

number of elemental variables, and thus each analysis requires careful interpretation, taking into account the mineralogy and the degree of trace-element homogeneity from grain to grain. As an example, when interpreting analytical results on chalcopyrite, one first determines the most common trace elements found in the mineral, based on a number of analyses, which in our case are Zn, Se, and In, all of which can occur as a solid solution in chalcopyrite (Cabri *et al.* 1985, Huston *et al.* 1995). Then, one examines analytical data with anomalously high concentrations of these or other elements, such as Sn. Because of the presence of stannite and cassiterite (Sn) and tetrahedrite–tennantite (Zn, Ag, Sb, As, Sn, Hg) in these samples, an analysis giving high Zn and Sn contents, coupled with low As and Hg, suggests a contribution from a subsurface inclusion of stannite rather than from tetrahedrite–tennantite, whereas high Sn alone suggests subsurface cassiterite.

Selected separates of pyrite and chalcopyrite (19 samples) from the different types of ore were analyzed by atomic absorption spectrophotometry (AAS) for Co, Ni and Mn. The purity of sulfide separates, hand-picked from bulk ore under a stereomicroscope, was checked by XRD analysis. No evidence of extra phases could be detected in the diffraction patterns of the analyzed minerals. In fact, no extra peaks of greater height than 3σ with respect to the background were observed. The AAS analyses were performed at the Dipartimento di Scienze della Terra of the University of Rome “La Sapienza”, Italy, using a Perkin Elmer 460 spectrophotometer.

MINERALOGY

Rubané ore

Rubané ore is composed of bands of chalcopyrite and pyrite (Fig. 3a), in some cases associated with cassiterite, alternating with dark gray to black layers of argillic schists ranging from millimeter to several centimeters thick. The observed minerals are, in order of decreasing abundance, chalcopyrite (about 30% of the bulk ore), two generations of pyrite (*i.e.*, pyrite I and pyrite II, representing about 5 and 15% of the bulk ore, respectively), cassiterite (10%, but present only in the RT ore), sphalerite (5%), tetrahedrite–tennantite (3%), k esterite (1%), two generations of arsenopyrite (*i.e.*, arsenopyrite I and arsenopyrite II, each 1%) and galena (1%). Abundant quartz and rare chlorite are gangue minerals, constituting about 30% of the bulk ore.

Chalcopyrite is the most abundant mineral in the sulfide-bearing layers, where it occurs as large lumps enclosing the other sulfides and sulfosalts. Chalcopyrite commonly infills fractures in pyrite II, representing in places the matrix of this latter sulfide (Fig. 3b). Chalcopyrite also occurs as exsolution-induced blebs in sphalerite. Pyrite I is less abundant than pyrite II and occurs as round sponge-like grains of variable size with corroded margins replaced by euhedral to subhedral

pyrite II. Pyrite is the most abundant sulfide in schist layers, especially black schists, where it forms monomineralic disseminations. Cassiterite constitutes mm-thick layers parallel to the rock schistosity in the RT ore. The cassiterite crystals are generally larger than the sulfide crystals, and have fractures mainly infilled by chalcopyrite. Sphalerite, which occurs as small irregular grains with chalcopyrite inclusions, is associated with galena, tetrahedrite–tennantite and k esterite, and may be included in large grains of chalcopyrite (Fig. 3c). Exsolution-induced blebs of k esterite may rim the sphalerite crystals (Fig. 3d). The minerals of the tetrahedrite–tennantite series, which mainly show a compositional range in the tennantite field, as determined by EPMA (see below), occur as irregular grains of variable size included by chalcopyrite. The minerals of the tetrahedrite–tennantite series may also infill fractures of pyrite II, along with sphalerite and galena. End-member tennantite occurs in pockets, and is partially replaced by arsenopyrite II, chalcopyrite and sphalerite (Fig. 3e). Members of the stannite–k esterite series, which are compositionally closer to the k esterite end-member, are relatively rare, forming exsolution-induced blebs in sphalerite (Fig. 3d), or are included in galena. Rare arsenopyrite I, which is associated with galena in the schists as disseminations of subhedral crystals of variable size (Fig. 3f), locally showing corroded margins, contains quartz or is replaced by chalcopyrite along fractures. Arsenopyrite II forms smaller subhedral crystals associated with tennantite (Fig. 3e). Galena, which is associated with sphalerite, and in some cases with the minerals of the tetrahedrite–tennantite series, is very rare, occurring as minute inclusions in chalcopyrite and infilling the fractures of pyrite II and quartz included by chalcopyrite.

Massive ore

Massive sulfide ore consists of finely banded sulfides (Fig. 4a), mainly pyrite and chalcopyrite, which are generally very fine-grained. Cassiterite grains some millimeters in diameter occur locally. In more detail, massive ore is composed of two generations of chalcopyrite (chalcopyrite I and chalcopyrite II: 45 and 5% of the bulk ore, respectively), two generations of pyrite (pyrite I and pyrite II: 5 and 15%, respectively), cassiterite (3%, but present only in the MS ore), two generations of sphalerite (sphalerite I and sphalerite II, 2%), stannite (1%), arsenopyrite, tetrahedrite–tennantite and galena (each of the last three <1%). The gangue minerals, which represent about 20% of the bulk ore, are composed of quartz, carbonates and rare chlorite.

Chalcopyrite I occurs as the matrix, locally replacing other minerals. Chalcopyrite I commonly infills fractures of pyrite and cassiterite. In contrast, chalcopyrite II is associated with carbonates and stannite. As observed in this deposit (Gaspar & Pinto 1993) and in other deposits of the Iberian Pyrite Belt (Garcia de Miguel

1990), pyrite I is present as characteristic relics of colloform and atoll structure (Fig. 4b) showing radial structures, which are typical of Kuroko-type deposits

(Leitch 1981). Pyrite II occurs as euhedral to subhedral crystals of variable size, replaced to a variable extent by chalcopyrite I. Pyrite II contains fractures filled by chal-

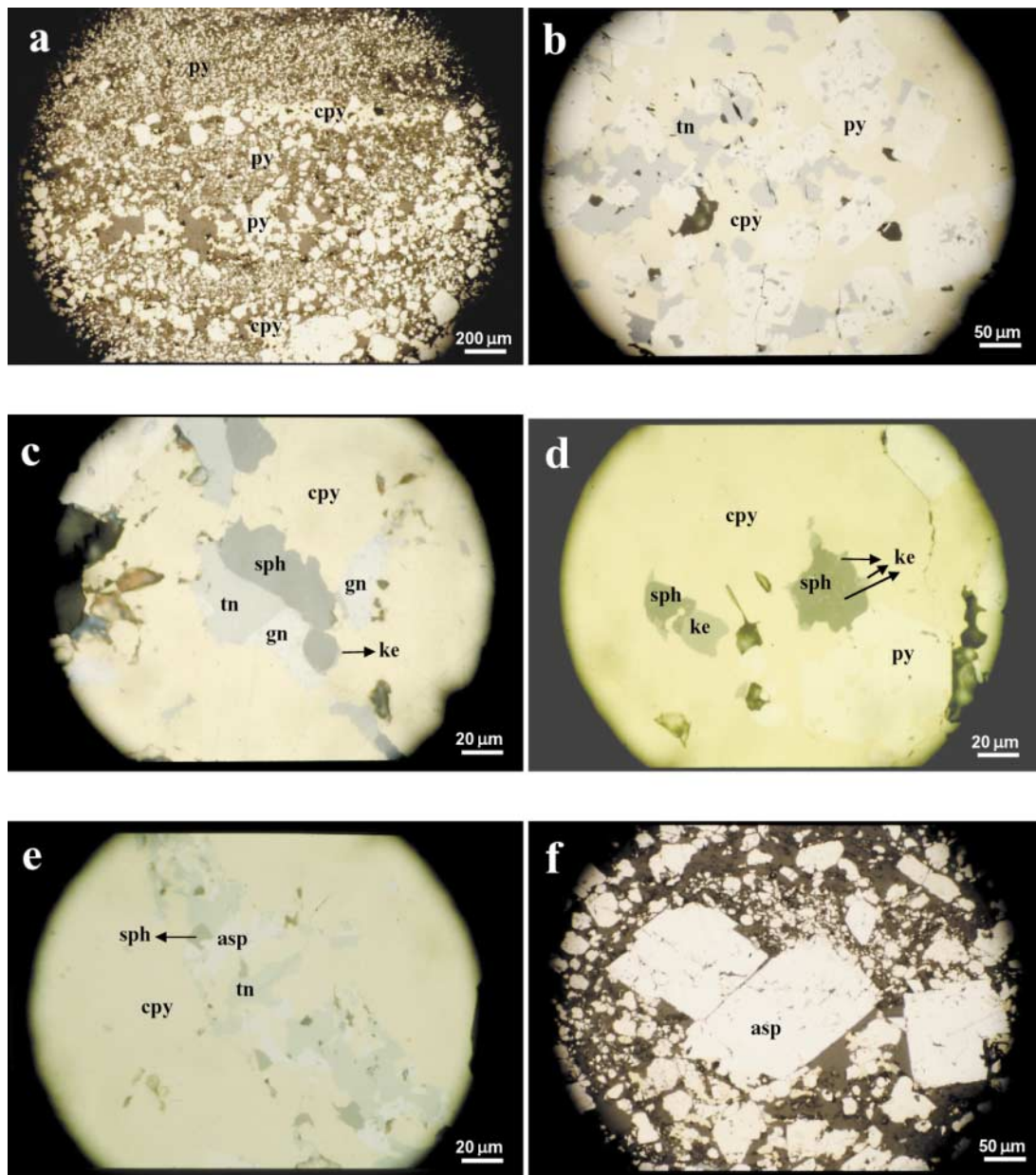


FIG. 3. Mineralogy of *rubané* ore (RC) of the Corvo deposit (microphotographs in reflected light, parallel nicols). a. Typical aspect of *rubané* ore, composed of bands of pyrite disseminated in black schists and bands of sulfides with dominant chalcopyrite (50 \times). b. Subhedral crystals of pyrite II replaced by tennantite and chalcopyrite (200 \times). c. Association of sphalerite rimmed by k esterite, tennantite and galena in a matrix of chalcopyrite (500 \times). d. Sphalerite with exsolution lamellae of k esterite in a matrix of chalcopyrite (500 \times). e. Tennantite, partially replaced by arsenopyrite II, chalcopyrite and sphalerite (500 \times). f. Subhedral crystals of arsenopyrite I of various size disseminated in black schists (200 \times).

copyrite I and, subordinately, sphalerite II, tetrahedrite and galena (Fig. 4c). Carbonate lumps may contain inclusions of pyrite II. Cassiterite forms lenses or nodules

of prismatic to subhedral crystals of cm to mm size, which may be fractured. In transmitted light, cassiterite shows concentric zoning from light yellow to dark red

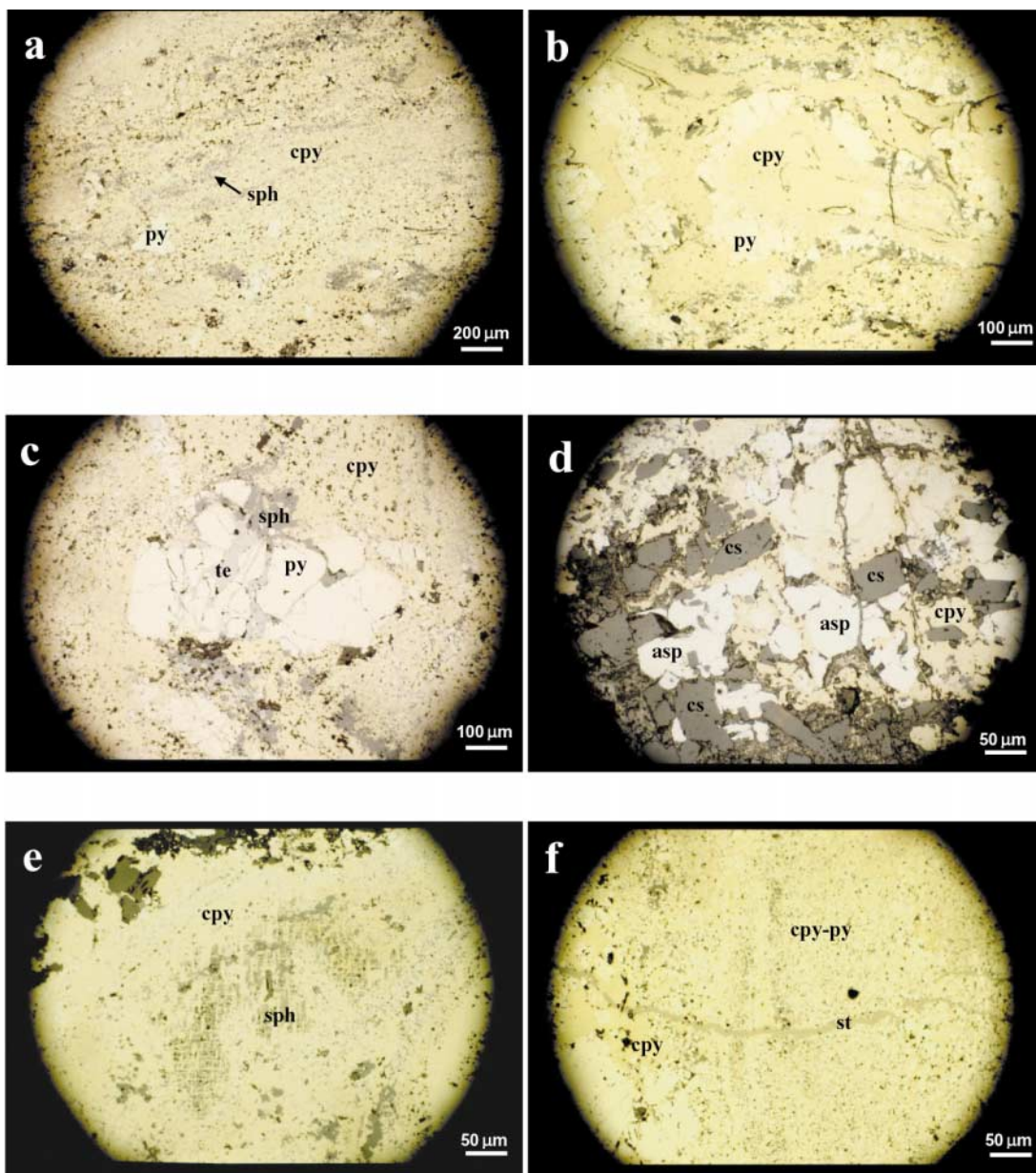


FIG. 4. Mineralogy of the massive ore (MS) of the Corvo deposit (microphotographs in reflected light, parallel nicols). a. Typical aspect of massive ore, composed of banded and fine-grained sulfides (mainly pyrite and chalcopyrite) (50 \times). b. Relics of pyrite I showing atoll and colloform structures in a matrix of chalcopyrite I (100 \times). c. Subhedral crystals of pyrite II with fractures infilled by tetrahedrite, sphalerite II and galena, in turn included in chalcopyrite I (100 \times). d. Subhedral prismatic crystals of cassiterite associated with arsenopyrite I in a matrix of chalcopyrite I (200 \times). e. Sphalerite I showing an advanced stage of selective replacement by chalcopyrite I (200 \times). f. Stannite veinlet cross-cutting bands of massive sulfide (200 \times).

in bands of variable intensity and size. This zoning correlates with chemical composition, as proven by electron-microprobe data and image analysis (Bonifazi & Serranti 1996). Cassiterite, which is mainly associated with arsenopyrite (Fig. 4d) or included in carbonate lumps, shows crystal fractures infilled by chalcopyrite I and pyrite II. Sphalerite I occurs as relics showing selective advanced replacement by chalcopyrite I (Fig. 4e). Sphalerite II is present as small grains associated with chalcopyrite in bands alternating with chalcopyrite bands. Along with tetrahedrite and galena, sphalerite II locally fills fractures in pyrite II (Fig. 4c). The minerals of the stannite–kësterite series, which are compositionally close to the stannite end-member, as determined by EPMA, occur as irregular grains generally larger than the kësterite crystals from the *rubané* ore. Stannite, which is commonly associated with carbonates in veinlets cross-cutting the mineralization (Fig. 4f), may also replace pyrite II or constitute the matrix for pyrite II and arsenopyrite. The latter sulfide is relatively rare, forming subhedral rhombic crystals of variable size, fractured and replaced by chalcopyrite I. Arsenopyrite generally includes or rims cassiterite (Fig. 4d). The very rare minerals of the tetrahedrite–tennantite series, which are compositionally close to the tetrahedrite end-member, as determined by EPMA, occur as small irregular grains within lumps of chalcopyrite I or, in some cases, infill the fractures of pyrite II crystals, together with sphalerite II and galena (Fig. 4c). Galena, which may include sphalerite II, also is very rare, forming very small grains hosted by chalcopyrite.

Paragenetic sequence

It is not easy to establish the paragenetic sequence of the Corvo mineralization because of the very complex structural and textural relationships among minerals, as usually observed in deposits of the Iberian Pyrite Belt (Garcia De Miguel 1990). However, we have schematically defined three stages on the basis of either characteristic minerals or typical structures and textures (Fig. 5). Stage I is characterized by the deposition of pyrite I and sphalerite I. Pyrite I shows typically atoll, colloform and radial structures, indicating its formation during rapid cooling of exhalative fluids at the contact with seawater (Garcia De Miguel 1990). With an increasing rate of volcanic exhalations and insulation of the external surface of the deposited massive sulfides, there was the deposition of cassiterite, arsenopyrite I and euhedral pyrite II, followed by sphalerite II, kësterite, tetrahedrite–tennantite, arsenopyrite II and galena. This stage is referred to the main stage of mineralization or Stage II. The last mineral deposited in this stage was abundant chalcopyrite I, which encloses, replaces and infills fractures of earlier sulfides. During Stage III, stannite, chalcopyrite II and carbonates were deposited in veinlets cross-cutting the orebody.

RESULTS OF EPMA AND MICRO-PIXE ANALYSES, WITH INTERPRETATION OF ELEMENT SITING

The results of EPMA and micro-PIXE analyses are presented in Table 2, where mean values of concentration of the elements detected are reported only if at least 50% of the measurement were greater than the minimum detection level (MDL). A comparison of element concentrations obtained by PIXE and EPMA shows good agreement, as already observed in other studies (*e.g.*, Campbell *et al.* 1990).

The trace elements monitored may result from stoichiometric or non-stoichiometric structural substitutions for major elements in a given mineral, or from the presence of mineral inclusions. The trace-element siting in the mineral structure is discussed here, because it may be critical for understanding the genesis of the ore (Huston *et al.* 1995). The distribution of the elements detected in minerals from *rubané* and massive ores also is discussed.

Cassiterite

A total of 88 EPMA analyses were carried out on cassiterite from MS and RT ores in order to evaluate elements usually substituting for Sn, such as Fe, Nb, Ta, Ti, W, Mn and Al (*e.g.*, Giuliani 1987, Izoret *et al.* 1985, Möller *et al.* 1988, Neiva 1996, Murciego *et al.* 1997). Cassiterite crystals display chemical zoning, with dark (Fe-rich) and light (Fe-poor) bands indicating repeated variations of the composition of the mineralizing fluids during the deposition of this mineral. Fe and W were

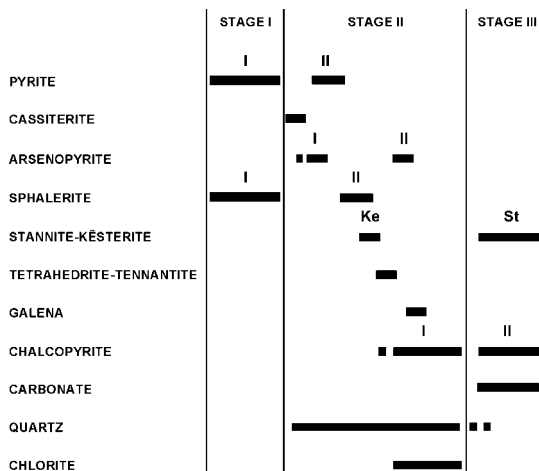


FIG. 5. Paragenetic sequence of the main mineral phases of the mineralization at Corvo.

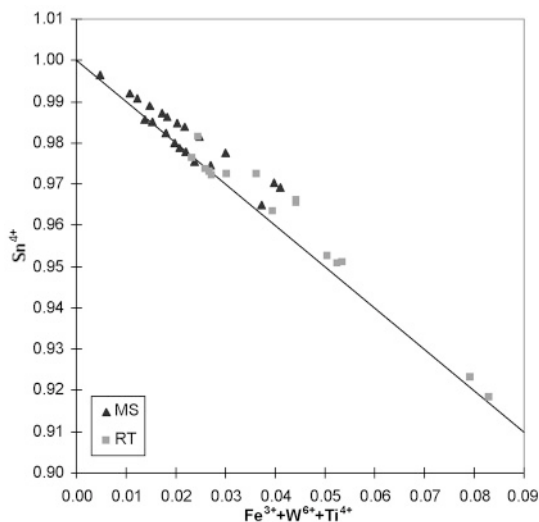


FIG. 6. Sn replacement by $\Sigma(\text{Fe} + \text{W} + \text{Ti})$ in cassiterite from massive sulfide (MS) and *rubané* tin (RT) ores of the Corvo deposit. The values represent the number of atoms per formula unit (*apfu*).

detected with similar ranges in both MS and RT cassiterite, whereas Ti was detected only in RT cassiterite. The presence of Ti in RT cassiterite may mean that very reduced fluids deposited this mineral, because Ti is mobile under very reduced conditions (Seifert *et al.* 1997). The abundance of the other elements was found to be below the detection limit, in agreement with the results of Neiva (1996) and Seifert *et al.* (1997) on cassiterite from the Corvo deposit. Fe^{3+} , W^{6+} and Ti^{4+} substitute for Sn^{4+} as follows: 1) Fe alone, 2) Fe + W, 3) Fe + Ti (only in the RT ore). In fact, in Figure 6 the points representing the sum of the three cations *versus* Sn lie along a line with slope of -1 , indicating the correct stoichiometry. Only Fe was detected in samples lying in the field above the line, showing that substitution of Fe^{3+} for Sn can give excess cations, in agreement with the observations by Möller *et al.* (1988). Figure 7 shows the correlation of Fe and W in samples where both were detected. It appears that all samples lie along or below the line $\text{W}:\text{Fe} = 0.5$. This value probably represents the upper limit of the $\text{W}:\text{Fe}$ ratio, indicating the presence of Fe_2WO_6 as solid solution in cassiterite crystals (Möller *et al.* 1988). In contrast, the diagonal line representing the atomic ratio $\text{W}:\text{Fe} = 1$ indicates the presence of ferberite as solid inclusions.

Micro-PIXE analyses show that cassiterite also contains traces of Cu, Zn, As, In, Sb, Ta and Pb. Ta likely occurs in the cassiterite structure because of the lack of Ta-bearing minerals. In is probably structurally bound, whereas Cu, Zn, As, Pb and Sb likely reflect the presence of subsurface inclusions of sulfides.

Chalcopyrite

No variation in major elements was found in this mineral from the MS, MC and RC ores on the basis of 57 EPMA analyses. In contrast, Sn content distinguishes the various ores, because RC and MC chalcopyrite contains more Sn than MS chalcopyrite.

Thirteen micro-PIXE analyses indicate trace amounts of Sn, Zn, Se and In in chalcopyrite. In particular, the distribution of Sn among the various ores obtained by EPMA analyses is confirmed. The largely variable concentrations (from ten to hundreds of ppm) of Sb, As, Hg, Ag, and Pb measured in two samples may indicate the presence of subsurface inclusions of tetrahedrite-tennantite and galena, respectively. Likewise, the presence of subsurface inclusions of stannite is considered to be likely in two samples that contain high Zn and Sn coupled with low As and Hg. In contrast, the moderate or low Zn and Sn contents in the other samples suggest substitution. Substitution is also probable in the case of In and Se. Indium, Sn and, possibly, Zn substitute for Fe, whereas Se substitutes for S. The In contents are similar to those (0.00–0.14 wt.%) measured by EPMA (Legendre 1994) in chalcopyrite from the Corvo orebody. The In contents are significantly higher than those in chalcopyrite from Australian VMS deposits (Huston *et al.* 1995), but they are in the range of those (up to 4,383 ppm) in chalcopyrite from the Kidd Creek deposit, Ontario (Cabri *et al.* 1985). The high levels of Se are similar to those in chalcopyrite from Cu-rich VMS deposits, where Se concentra-

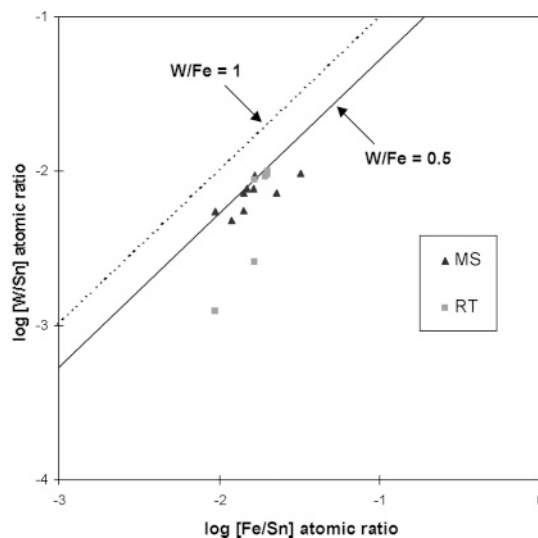


FIG. 7. The correlation between $\log[\text{W}/\text{Sn}]$ and $\log[\text{Fe}/\text{Sn}]$ in cassiterite from massive sulfide (MS) and tin-bearing *rubané* (RT) ores of the Corvo deposit.

TABLE 2. COMPOSITION OF MINERALS FROM THE CORVO OREBODY, PORTUGAL

Cassiterite: EPMA data (wt.%)					Chalcopyrite: EPMA data (wt.%)											
ore type	SnO ₂	FeO	WO ₃	TiO ₂	ore type	Cu	Fe	Sn	S							
MS n = 58	98.45 ± 0.86 97.00–99.92	0.99 ± 0.51 0.45–2.19	- <0.08–1.40	- <0.03	MS n = 12	34.22 ± 0.47 33.32–34.60	30.39 ± 0.24 29.93–30.63	- <0.02–0.03	35.05 ± 0.33 34.77–35.66							
RT n = 30	97.19 ± 1.00 94.89–98.45	1.05 ± 0.56 0.53–2.18	- <0.08–1.50	- <0.03–4.06	MC n = 20	34.48 ± 0.16 34.25–34.69	30.17 ± 0.25 29.76–30.58	0.07 ± 0.03 0.04–0.12	34.91 ± 0.11 34.74–35.05							
MDL	-	0.02	0.08	0.03	RC n = 25	34.35 ± 0.15 34.08–34.56	30.16 ± 0.24 29.61–30.44	0.08 ± 0.03 0.06–0.16	34.93 ± 0.31 34.64–35.48							
MnO, Nb ₂ O ₅ , Ta ₂ O ₅ are present in concentrations less than the minimum detection-limit, MDL (0.02, 0.03 and 0.07%, respectively).					MDL											
MDL					MDL											
Cassiterite: PIXE data (ppm)								Chalcopyrite: PIXE data (ppm)								
ore type	Cu	Zn	As	In	Sb	Ta	Pb	ore type	Sn	Zn	Se	In				
MS n = 7	205 36–919	50 10–136	9 <2.6–41	284 203–357	- <105–145	53 37–91	11 <7–18	MS n = 3	434 214–819	151 124–178	253 124–327	321 173–434				
RT n = 4	18 10–33	- <3.6–6	4 3–6	309 180–394	- <105–243	45 <16–98	13 <7–18	MC n = 4	594 233–955	142 141–143	190 115–330	176 49–366				
MDL	4	3.6	2.6	95	105	16	7	RC n = 6	1072 754–1385	248 131–423	278 158–456	115 39–220				
Zr and Nb are present in concentrations less than the minimum detection-limit, MDL (3.9 and 4.6 ppm, respectively).								MDL								
MDL								MDL								
Pyrite: EPMA data (wt.%)				Stannite: EPMA data (wt.%)												
ore type	Fe	Cu	S	ore type	Cu	Fe	Sn	Zn	S							
MS n = 20	46.76 ± 0.14 46.47–46.95	0.05 ± 0.02 0.03–0.08	53.20 ± 0.17 52.99–53.43	MS n = 19	28.91 ± 1.01 26.07–29.84	11.10 ± 1.84 9.11–15.26	20.27 ± 2.21 23.17–29.75	3.21 ± 2.21 1.91–11.74	29.15 ± 0.64 28.47–31.33							
MC n = 17	46.59 ± 0.32 46.11–47.09	- <0.02–0.08	53.27 ± 0.34 52.78–53.81	MC n = 13	29.31 ± 0.63 28.13–29.97	10.59 ± 1.12 8.16–11.67	26.98 ± 0.60 26.12–27.88	4.06 ± 1.79 1.89–6.38	28.98 ± 0.85 27.74–30.09							
RC n = 30	46.64 ± 0.18 46.28–46.96	- <0.03–0.29	53.04 ± 0.29 52.48–53.55	RC n = 20	28.07 ± 0.64 27.11–29.16	3.24 ± 0.51 2.37–4.04	28.15 ± 0.67 26.58–28.98	12.41 ± 0.62 11.20–13.65	28.11 ± 0.53 27.09–29.05							
MDL	-	0.03	-	MDL												
Co, Ni and As are present in concentrations less than the minimum detection-limit, MDL (0.03, 0.03 and 0.02%, respectively).				MDL												
MDL				MDL												
Pyrite: PIXE data (ppm)								Stannite-k�esterite: PIXE data (ppm)								
ore type	Ni	Cu	Zn	As	Se	Sn	Pb	In	ore type	Se	Ag	Cd	In	Sb	Hg	Pb
MS n = 4	<21–27	298 102–463	28 9–55	11 <4–26	202 23–609	159 <11–232	<33	<9–11	MS n = 2	510 419–600	39 29–49	158 107–208	675 452–897	403 <78–244	403 317–489	176 <29–325
MC n = 4	<21–28	460 216–703	44 23–79	182 15–531	<3.6–451	105 12–371	<33–50	<9–18	MC n = 2	994 531–1457	319 297–340	173 150–196	1077 984–1170	1663 634–2692	530 525–535	65 58–72
RC n = 8	<21–89	202 94–408	38 16–74	238 25–590	<3.6–675	118 <11–24	<33–403	<9–11	MDL	6	16	39	63	78	22	29
MDL	21	10	7	4	3.6	11	33	9	MDL							
Chlorite: EPMA data (wt.%)																
ore type	SiO ₂	Al ₂ O ₃	FeO	MgO	H ₂ O											
MC n = 12	21.73 ± 0.01 21.72–21.74	23.59 ± 0.76 22.59–24.39	45.81 ± 0.10 45.69–45.92	0.71 ± 0.02 0.69–0.73	8.34 ± 1.00 7.48–9.75											
RT n = 10	22.11 ± 0.07 22.05–22.21	25.90 ± 0.05 25.84–25.95	40.91 ± 0.03 40.88–40.94	2.95 ± 0.04 2.89–2.99	8.13 ± 0.08 8.08–8.25											

The EPMA data presented are the mode, the standard deviation, the range of concentrations encountered, and the minimum detection limit (MDL). The PIXE data presented are the mode, the range of concentrations encountered, and the minimum detection limit (MDL). The number of analyses *n* also is shown.

TABLE 2 (continued). COMPOSITION OF MINERALS FROM THE CORVO OREBODY, PORTUGAL

Tetrahedrite-tennantite: EPMA data (wt.%)									
ore type	Cu	Zn	Fe	Ag	Sb	As	Sn	Bi	S
MS <i>n</i> = 20	37.25 ± 0.33 36.63–37.62	5.62 ± 0.35 5.13–6.22	2.17 ± 0.41 1.75–2.83	1.20 ± 0.19 0.83–1.17	28.63 ± 0.57 28.08–29.73	0.75 ± 0.18 0.58–1.13	- <0.02	- <0.05–0.08	24.49 ± 0.46 23.78–24.97
MC <i>n</i> = 15	34.69 ± 0.78 33.47–36.04	6.99 ± 1.91 3.54–9.47	3.27 ± 0.38 2.55–3.75	3.15 ± 1.08 1.56–4.84	28.03 ± 1.40 25.11–29.41	- <0.03–2.40	- <0.02	- <0.05–0.44	23.48 ± 0.64 22.85–24.54
RC <i>n</i> = 42	41.64 ± 1.80 37.15–43.40	4.53 ± 0.69 3.28–5.70	3.82 ± 0.81 1.09–5.37	- <0.03–0.34	9.47 ± 7.40 2.01–27.03	13.83 ± 5.03 0.68–19.44	- <0.02	- <0.05–1.36	26.99 ± 1.10 23.67–28.28
MDL	-	-	-	0.03	-	0.03	0.02	<0.05	-

Tetrahedrite-tennantite: PIXE data (ppm)									
ore type	Ni	Se	Ag	Cd	In	Sn	Hg	Bi	As
MS td <i>n</i> = 1	-	1201	11010	257	178	753	1398	474	5270
MC td <i>n</i> = 1	-	1016	35988	473	86	4784	3132	304	13580
MDL	-	12	19	23	43	115	187	22	14
RC tn <i>n</i> = 4	893 <695–1369	657 538–800	718 537–972	108 88–139	34 23–55	644 <45–619	644 570–723	321 223–400	-
MDL	695	31	36	11	20	45	72	22	-

Symbols used: td: tetrahedrite, tn: tennantite.

Sphalerite: EPMA data (wt.%)							
ore type	Zn	Fe	Cu	Cd	In	Hg	S
MS <i>n</i> = 19	64.75 ± 0.60 63.76–65.70	1.39 ± 0.46 0.81–2.51	0.07 ± 0.01 0.08–0.78	0.07 ± 0.01 0.06–0.09	0.10 ± 0.02 0.07–0.14	0.21 ± 0.03 0.18–0.26	32.66 ± 0.49 31.72–33.42
MC <i>n</i> = 26	63.61 ± 0.67 62.90–64.69	2.30 ± 0.46 1.53–2.91	0.45 ± 0.29 0.14–1.02	0.20 ± 0.06 0.07–0.27	0.06 ± 0.02 0.03–0.08	0.16 ± 0.04 0.11–0.24	32.81 ± 0.19 32.48–33.17
RC <i>n</i> = 27	64.93 ± 0.68 63.29–66.02	1.15 ± 0.50 0.66–2.43	0.45 ± 0.26 0.24–0.88	0.09 ± 0.06 0.04–0.25	0.05 ± 0.03 0.02–0.10	0.18 ± 0.04 0.13–0.24	32.71 ± 0.23 32.20–32.97
MDL	-	-	0.02	0.02	0.02	0.10	-

The concentration of Mn and Sn is below the MDL (0.02 wt.%).

Arsenopyrite: EPMA data (wt.%)							
ore type	Fe	Co	As	Sb	S	Ni	Sn
MS <i>n</i> = 28	33.93 ± 0.45 33.01–34.58	0.41 ± 0.26 0.04–0.92	44.37 ± 0.90 42.05–45.84	0.09 <0.02–0.95	20.90 ± 0.54 20.09–22.20	- <0.03	- <0.02
RC <i>n</i> = 20	34.25 ± 0.34 33.64–34.87	- <0.03–0.45	43.89 ± 0.73 42.32–44.90	- <0.02–1.01	21.23 ± 0.66 19.84–22.68	- <0.03	- <0.02
MDL	-	0.03	-	0.02	-	0.03	0.02

The concentration of Ni and Sn is below the MDL (0.03 and 0.02 wt.%, respectively).

tions usually exceed the values measured in pyrite (Huston *et al.* 1995). A comparison of the composition of chalcopyrite from the ore samples studied shows significant patterns of distribution for Sn, In and Se. In fact, the lower concentration of Sn measured in MS chalcopyrite may be explained by the later formation of this sulfide with respect to cassiterite, which left the fluids relatively depleted in Sn. The In content of chalcopyrite samples decreases from MS to MC and RC. Because this distribution parallels the decreasing abundance of Cu in the three ores, there is a suggestion that In and Cu were closely associated. The Se content of chalcopyrite samples decreases from RC through MS to MC. Because Se generally concentrates in chalcopyrite from the Cu-rich stringer zone and the lower part of massive ore (Huston *et al.* 1995), the observed distribution of Se suggests that RC chalcopyrite was deposited in a deeper zone than chalcopyrite from the massive ores, assuming a single line of descent for the Corvo mineralizing fluids. This, in turn, may mean that the *rubané* ore was originally located below the massive ore.

Pyrite

Results of 67 EPMA analyses suggest that this mineral is compositionally similar in the MS, MC and RC ores. Sixteen micro-PIXE analyses of pyrite from these ores show that it generally contains measurable amounts of Ni, Cu, Zn, As, Se, Sn and Pb, whereas In was detected only in a few samples at very low concentrations, close to the MDL. According to Huston *et al.* (1995), the presence of Cu, Zn and Pb may be explained by subsurface inclusions of chalcopyrite, sphalerite and galena, respectively. In contrast, As, Ni and Se may substitute for Fe and S in the structure. The siting of In cannot be determined. The Ni and In contents are similar to those in pyrite from Australian and Canadian VMS

deposits (Huston *et al.* 1995, Cabri *et al.* 1985). Sn is probably structurally bound, considering that Sn levels up to 3,000 ppm in pyrite from the Kidd Creek deposit are explained by solid solution of Sn in the structure (Cabri *et al.* 1985). Moreover, because the concentrations of Sn and Cu in pyrite do not correlate positively, inclusions of stannite can be excluded. The comparison of the composition of pyrite from the *rubané* and massive ores shows the antithetic behavior of As and Sn, as the former decreases and the latter increases from the RC through the MC to the MS ore. The distributions of As and Sn in pyrite parallel the decrease of As and the increase of Sn abundance in the corresponding bulk ores, respectively, thus reflecting the concentrations of these elements in the fluids. Se content decreases from MS through RC to MC pyrite.

Tetrahedrite–tennantite

Results of 77 EPMA analyses show distinct compositions for minerals of this series from the MS, MC and RC ores (Fig. 8). In fact, the minerals of the tetrahedrite–tennantite series in the massive ores are compositionally close to the tetrahedrite end-member (>90% of that component), whereas the corresponding minerals from the RC ore are generally close to the tennantite end-member (55 to 95% of that component). Moreover, the Ag contents distinguish the three types of ore, because Ag is lower in RC tennantite (<0.03–0.34 wt%) and higher in tetrahedrite from the massive ores (MS ore 1.20 ± 0.19 wt%, MC ore 3.15 ± 1.08 wt%). This fact may have special significance in connection with the genetic relationships between *rubané* and massive ore. In fact, because both Ag and Sb sulfosalts are associated with late fluids compared to As sulfosalts (*e.g.*, Bortnikov *et al.* 1993), it is possible that Ag-rich tetrahedrite from the massive ores was deposited by late fluids, probably characterized by lower temperatures compared to fluids forming tennantite in *rubané* ore. Such a hypothesis, in addition to evidence that stockwork ores of the IPB deposits are usually depleted in Sb and Ag compared to those lying above massive ore (Marcoux *et al.* 1996), suggests a similarity between *rubané* and stockwork ore.

Micro-PIXE analyses of RC tennantite and tetrahedrite from massive ores reveal concentrations of the following elements: Ni (only in RC tennantite), Se, Ag, Cd, In, Sn, Hg, Bi and As (this latter obviously derived from tetrahedrite, being a major element in the tennantite component). In particular, the distribution of Ag among the various ores obtained by EPMA analyses is confirmed. The high concentrations of Sn (up to 4,784 ppm) suggest subsurface inclusions of a Sn-bearing mineral, because Sn contents measured by EPMA are lower than 0.02%. The other elements detected are structurally bound, considering that the general formula of the tetrahedrite–tennantite series is $(\text{Cu,Ag})_{10}(\text{Fe,Zn})_2(\text{Sb,As})_4\text{S}_{13}$, and chemical studies demonstrate limited

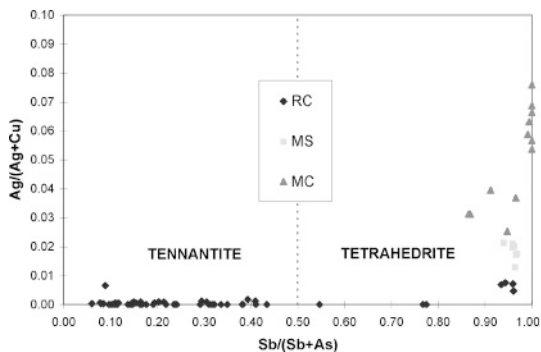


FIG. 8. Chemical composition of the members of the tetrahedrite–tennantite series ($\text{Cu}_{12}\text{Sb}_4\text{S}_{13}$ – $\text{Cu}_{12}\text{As}_4\text{S}_{13}$) from massive sulfide (MS and MC) and *rubané* (RC) ores of the Corvo deposit.

substitution of Cu, Hg, Cd, Pb for Fe or Zn, Bi, Te for Sb or As, and Se for S (Seal *et al.* 1990). Ni and In probably substitute for Fe. Tetrahedrite from massive ores is generally enriched in most trace elements with respect to RC tennantite, probably reflecting correspondingly higher concentrations in the mineralizing fluids of the massive ores.

Stannite–k esterite

Results of fifty-two EPMA analyses show a wide compositional range for minerals of this series from the MS, MC and RC ores. Stannite (Fe-rich member) occurs in the massive ores (76 and 81% of stannite end-member in the MC and MS ores, respectively) and is characteristic of stage III, whereas k esterite (Zn-rich member) is present in the *ruban * ore (77% of that end-member) and deposited during stage II (Fig. 9).

The trace elements detected in stannite by microPIXE analyses of material from massive ores are Se, Ag, Cd, In, Sb, Hg and Pb. These elements may be present in the structure, except for Sb and Pb, the erratic concentrations of which may be explained by subsurface inclusions of an Sb-bearing mineral and galena, respectively. Indium probably substitutes for Sn, coupled with Zn and Fe substituting for Cu (Shimizu *et al.* 1986). The In contents are similar to those (0.00–2.04 wt.%) reported by Legendre (1994) for the same minerals from the Corvo orebody. Although very few

PIXE analyses were made, Se, Ag, In and Hg are probably enriched in RC k esterite in contrast to MS stannite.

Sphalerite

A total of 72 EPMA analyses were carried out on this mineral from the MS, MC and RC ores. Unlike Mn and Sn, undetected at MDL (0.02 wt.%), Fe, Cd, Cu, Hg and In were measurable, compensating the Zn deficiency compared to the theoretical formula. These elements are very likely structurally bound. In fact, Fe and Cd substitution for Zn is well known, and the low and uniform levels of Cu suggest the existence of a solid solution toward CuS (Kojima & Sugaki 1985). Concerning Hg and In, Barbanson *et al.* (1985) have documented the existence of a (Zn,Hg)S solid solution, and Johan (1988) and Patrick & Dorling (1991) have proposed that In coupled with Cu substitute for Zn: $\text{Cu}^{2+} + \text{In}^{3+} = 2 \text{Zn}^{2+}$. The In contents are lower than those (up to 5.45 wt.%) measured by Legendre (1994) for sphalerite from the Corvo orebody. A comparison of sphalerite compositions from the various types of ore shows significant distributions for In, Fe and Cd. The distribution of In is particularly interesting because sphalerite is the main carrier of In at Corvo. The In content decreases from MS to MC and RC ores. This distribution, which parallels the pattern of cassiterite abundance in the same ores, suggests some links between In and the Sn mineralization. From Figure 10, it seems that Fe and Cd have a similar behavior, decreasing from MC to MS and RC sphalerite. With respect to Fe, this distribution may be consistent with maximum activity of Fe in the pyrite-rich MC ore.

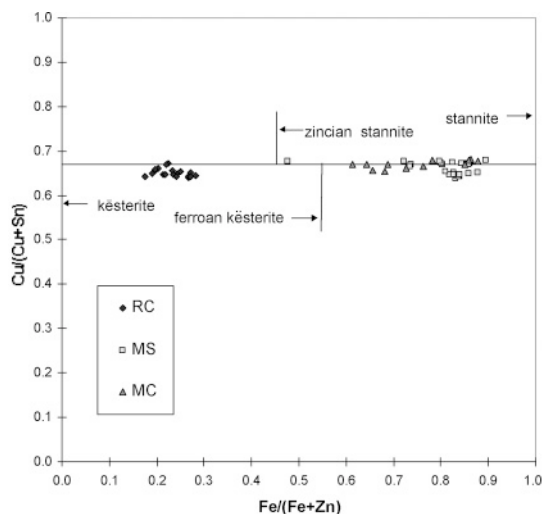


FIG. 9. Chemical composition of minerals in the stannite–k esterite series ($\text{Cu}_2\text{SnFeS}_4 - \text{Cu}_2\text{SnZnS}_4$) from massive sulfide (MS and MC) and *ruban * (RC) ores of the Corvo deposit, plotted in the classification diagram of Petruk (1973).

Arsenopyrite

Results of 48 EPMA analyses on arsenopyrite from the RC and MS ores show a small deficiency in As and

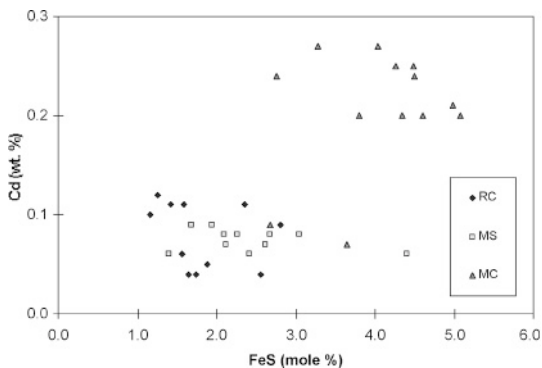


FIG. 10. Plot of FeS versus Cd content in sphalerite from massive sulfide (MS and MC) and *ruban * (RC) ores of the Corvo deposit.

Fe and an excess in S, compared with the theoretical formula, as usually observed in natural arsenopyrite (Kretschmar & Scott 1976). Among trace elements, only Co and Sb were detected above the MDL; they are probably present in substitution for As and Fe, respectively. A comparison of mineral compositions from the two types of ore shows that MS arsenopyrite contains higher As, Co and Sb than RC arsenopyrite, which, in contrast, is richer in Fe and S. Moreover, because the same compositional difference has been observed between arsenopyrite from the massive ore and the stockwork in other IPB deposits (Marcoux *et al.* 1996), this finding may be significant for the stratigraphic meaning of the *rubané* ore, as will be discussed later.

Chlorite

Relatively few EPMA analyses of chlorite from MC and RT ores were made. On the basis of its chemical composition, chlorite can be classified as high-Fe chamosite. A comparison of the mineral's composition from the two ores shows that RT chlorite contains more Mg and Al than MC chlorite, which, in contrast, contains more Fe. This latter feature is consistent with maximum activity of Fe in the MC fluids depositing pyrite-rich ore.

RESULTS OF AAS ANALYSES

The AAS analyses for Co, Ni and Mn in chalcopyrite separates and intimate mixtures of pyrite and chalcopyrite from the RC, MS and MC ores are given in Table 3. The average Co, Ni and Mn contents are lower

TABLE 3. Co, Ni AND Mn CONTENTS, AS DETERMINED BY AAS IN INTIMATE MIXTURES OF PYRITE (py) AND CHALCOPYRITE (cpy) AND IN PURE CHALCOPYRITE SEPARATES OF DIFFERENT ORE-TYPES

	Co	Ni	Co/Ni	Mn		Co	Ni	Co/Ni	Mn
	RC (cpy-py)					MC (py-cpy)			
C-2-1	57	20	2.85	41	AC-2	145	55	2.64	75
C-3-1	29	20	1.45	28	AC-3	147	37	3.97	47
C-4-1	33	16	2.06	24	AC-4	72	52	1.38	75
C-5-1	42	17	2.47	14	AC-5	104	15	6.93	47
mean	40	18	2.21	27	AC-6	195	25	7.80	167
s.d.	12	2	0.60	11	AC-7	511	42	12.17	102
					AC-10	99	46	2.15	169
					mean	182	39	5.29	97
					s.d.	151	14	3.88	52
	MS (cpy-py)					MC (cpy)			
C-10-1	385	66	5.83	38	AC-1	17	12	1.42	132
C-14-1	185	49	3.78	181	AC-7	17	10	1.70	129
C-15-1	80	34	2.35	60	AC-10	20	15	1.33	162
mean	217	50	3.99	93	mean	18	12	1.48	141
s.d.	155	16	1.75	77	s.d.	2	3	0.19	18

Concentrations are expressed in ppm.

in RC ore than in massive ores, which show similar contents if the standard deviations are considered. Because Mn is an element generally concentrated in late fluids, there is a suggestion that the fluids depositing the massive ores were later than the *rubané*-depositing fluids, in the hypothesis of a single line of descent. Moreover, considering the composition of pure chalcopyrite from the MC ore with respect to the composition of mixtures of pyrite and chalcopyrite from the same ore, there is an indication that the bulk of Co and Ni is contained by pyrite, as is usually observed in other instances of mineralization, whereas the bulk of the Mn is concentrated in chalcopyrite. This latter feature is consistent with the fact that Mn usually concentrates in late fluids, and chalcopyrite was deposited after pyrite.

The average Co:Ni ratio of the RC ore is lower than that of the massive ores. All these values fall in the range (0.22–24.23) reported by Marcoux *et al.* (1996) for pyrite from other IPB deposits.

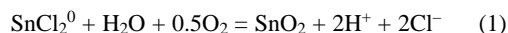
DISCUSSION

Physical-chemical conditions of ore formation

Information on temperature of the mineralizing fluids may be obtained by considering the composition of the minerals. In this view, using the geothermometer based on the composition of arsenopyrite (Kretschmar & Scott 1976), temperatures of 325–375°C and 340–400°C were calculated for RC (31.45 ± 0.74 atom % As) and MS (31.87 ± 0.80 atom % As) ores, respectively (Fig. 11). However, given the uncertainties of this method, there is no significant difference between the two types of ore. The temperature ranges may be reasonable, considering both the volcanogenic nature of the Corvo deposit and early crystallization of arsenopyrite in stage II. Additional information is provided by the application of the geothermometer based on the composition of the sphalerite–kësterite pair (Nakamura & Shima 1982, Shimizu & Shikazono 1985). In fact, temperatures of 329, 246 and 216°C can be calculated for the crystallization of these minerals in the RC, MC and MS ores, respectively. The temperature calculated for RC ore is consistent with that calculated for the same ore using arsenopyrite, considering that kësterite and sphalerite were deposited after arsenopyrite. The temperatures calculated for MC and MS ores are realistic, assuming that sphalerite underwent re-equilibration in stage III, during which stannite was deposited. Because stage-III temperatures are lower than those of stage II, it seems that temperature decreases with evolution of the mineralizing process. Moreover, considering the temperatures calculated for arsenopyrite, it is possible to estimate the values of $\log a(S_2)$ from the plot of Figure 11. Therefore, it is apparent that $\log a(S_2)$ ranged from –12 to –7 and from –12.5 to –7.5 during the crystallization of RC and MS arsenopyrite, respectively. In addition, because the diagrams of phase relationships

for the system Fe–Zn–S (Barton & Toulmin 1966, Scott & Barnes 1971) and for the system Fe–As–S (Kretschmar & Scott 1976) can be superimposed (as suggested by Scott 1983), we plotted in Figure 11 the isopleth (in mole % FeS) corresponding to the FeS content in RC sphalerite (2.02%). Considering the temperature calculated above for this sulfide, it appears that $\log a(\text{S}_2)$ was about -8 in stage II and sphalerite is not in equilibrium with arsenopyrite and pyrite, because sphalerite coexisting with these two minerals is expected to contain about 10 or more mole % FeS (Scott 1983). This inference is in agreement with the fact that the three sulfides were not deposited simultaneously. Further information on temperature of the fluids can be obtained from the composition of chlorite. In fact, the proportion of Al atoms in the tetrahedral position ($^{\text{IV}}\text{Al}$) in chlorite correlates positively with temperature (Cathelineau & Nieva 1985). Therefore, on the basis of the $^{\text{IV}}\text{Al}$ contents in MC and RT chlorite (3.10 and 3.19 atoms per formula unit, respectively), a temperature of about 350°C can be calculated for MC and RT ores. This temperature can be considered realistic, because it is similar to temperatures obtained by other methods.

In addition to temperature, oxygen fugacity is considered a key factor in the evolution of fluids forming cassiterite–sulfide deposits (Heinrich & Eadington 1986). In fact, thermodynamic calculations indicate that tin is transported in hydrothermal solutions mostly as reduced Sn^{2+} chloro complexes, for example SnCl_2^0 , rather than as Sn^{4+} thio- or hydroxy-chloro complexes. Precipitation of cassiterite involves an oxidation to Sn^{4+} :



and, therefore, depends critically on the oxygen fugacity (Heinrich & Eadington 1986, Patterson *et al.* 1981, Taylor & Wall 1993). Using an average temperature of 350°C and considering the association of sulfides and cassiterite, it is possible to evaluate from Figure 12 that during stage II, $\log a(\text{O}_2)$ was first about -36 , as required for the stability of cassiterite, then it ranged between -26 and -29 , considering the stability field of pyrite and the absence of pyrrhotite in the mineralization.

The range in pH, estimated from the stability field of chlorite and white mica, was between 3.4 and 4.9 (Patterson *et al.* 1981).

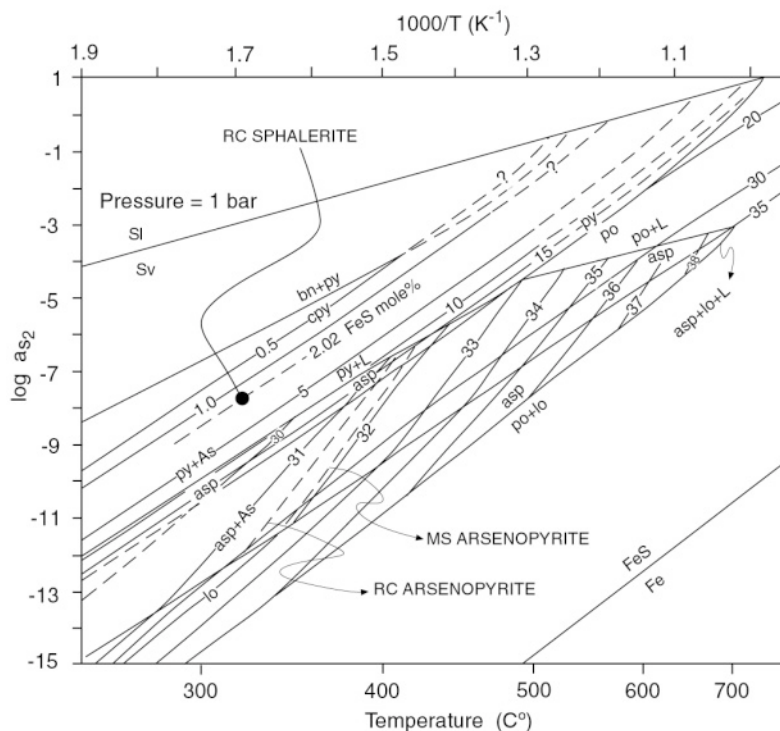


FIG. 11. Temperature versus $\log a(\text{S}_2)$ diagram showing concentration lines for As content (atom. %) in arsenopyrite and FeS content (mole %) in sphalerite (after Kretschmar & Scott 1976, Scott 1983). The RC and MS lines represent the arsenopyrite composition of the *rubané* and massive ores, respectively. The symbol (•) indicates the composition of sphalerite from *rubané* (RC) ore of the Corvo deposit, considering the FeS content in sphalerite and calculated temperature.

Origin of the sulfides

On the basis of the trace–element concentrations in the sulfides studied, some indications of the nature of the Corvo mineralizing fluids can be obtained. In this regard, we consider the In and Sn contents as well as the Se/S, Co/Ni and Zn/Cd values. The In contents of stannite, sphalerite, chalcopyrite and tetrahedrite–tennantite indicate a magmatic signature of the mineralizing fluids, being similar to the concentrations in ores deposited by high-temperature Cu-rich fluids with a magmatic contribution (Schwarz-Schampera & Herzig 1997). The In contents are higher than those detected in other IPB deposits (Marcoux *et al.* 1996). Indium is an element typical of a magmatic affiliation (Schwarz-Schampera & Herzig 1997). The fact that the Corvo mineralization has the highest contents among those of the IPB deposits suggests that the Corvo fluids were dominantly magmatic. Considering the distribution of In in the different types of ore, it appears that the In contents are usually higher in MS ore compared to MC and RC ores, confirming the association of this element with Cu and Sn, both being enriched in MS ore. The high levels of Sn in chalcopyrite indicate relatively reduced conditions of the mineralizing fluids, because Sn can best be transported in relevant quantities under reducing conditions and at high temperatures (Eugster 1986). The concentrations of Sn in pyrite are also consistent with the reduced nature of the fluids, as Sn is usually more enriched in pyrite from reduced or Cu-rich deposits than from oxidized or Zn-rich deposits (Huston *et al.* 1995).

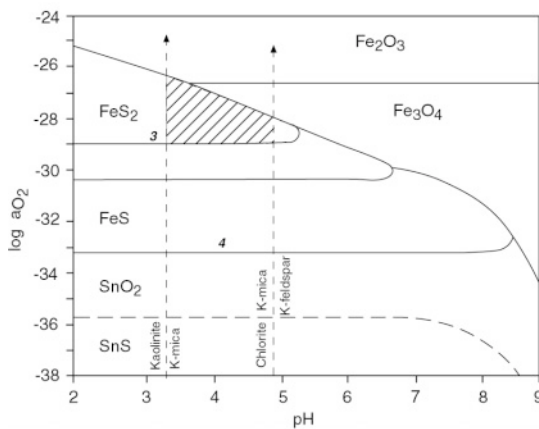


FIG. 12. pH – $\log a(\text{O}_2)$ diagram at $T = 350^\circ\text{C}$ (after Patterson *et al.* 1981). Curve 3 refers to the stability of arsenopyrite with respect to pyrite + As, whereas curve 4 refers to arsenopyrite stability with respect to pyrrhotite + löllingite. The dashed area defines the probable conditions of formation of *rubané* and massive ores of the Corvo deposit.

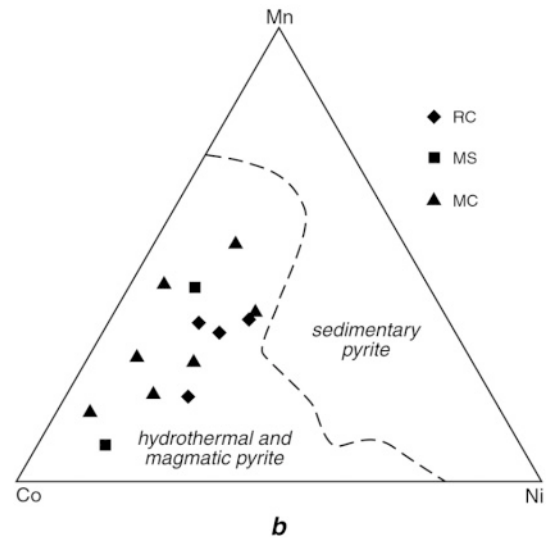


FIG. 13. Plot of the Co, Ni and Mn contents in mixtures of pyrite and chalcopyrite from ore types of the Corvo deposit. Reference fields for pyrite of various origins (after Udubaşa 1984) are shown for comparison.

Further evidence in favor of a dominantly magmatic signature of the fluids is provided by the Se/S values of pyrite ($\bar{x} = 3 \times 10^{-4}$), which are similar to the ratio of magmatic rocks ($5\text{--}20 \times 10^{-5}$) and quite distinct from the Se:S ratio of seawater ($2\text{--}10 \times 10^{-8}$; Huston *et al.* 1995). The average Zn/Cd values of sphalerite from MS (869), MC (313) and RC (696) ores also are consistent with a volcanogenic origin of the Corvo deposit (Xuexin 1984). This origin is also indicated by the Co, Ni and Mn contents in pyrite (Fig. 13; Udubaşa 1984), as well as the Co/Ni values of pyrite and chalcopyrite, which are similar to those of analogous sulfides from other VMS deposits (Fig. 14; Bajwah *et al.* 1987, Brill 1989).

The magmatic origin of sulfides may find support in preliminary results of the S-isotope composition of a few samples of intimate mixtures of pyrite and chalcopyrite from these ores. In fact, the overall $\delta^{34}\text{S}$ (CDT) ranges from -3.8 to $+5.0\text{‰}$ (V. Ferrini, unpubl. data), with no significant difference among the four ores. This range of $\delta^{34}\text{S}$, which falls within a wider range of values (-34 to $+15\text{‰}$) for sulfides from several IPB deposits (Velasco *et al.* 1998), overlaps the range for magmatic sulfur ($\pm 5\text{‰}$).

Origin of the cassiterite

Cassiterite from the Corvo orebody is similar to cassiterite from VMS deposits with respect to Nb, Ta and Zr contents, which are usually lower than those of cassiterite from granite-related deposits (Hennigh & Hutchinson 1997). However, cassiterite from Corvo is

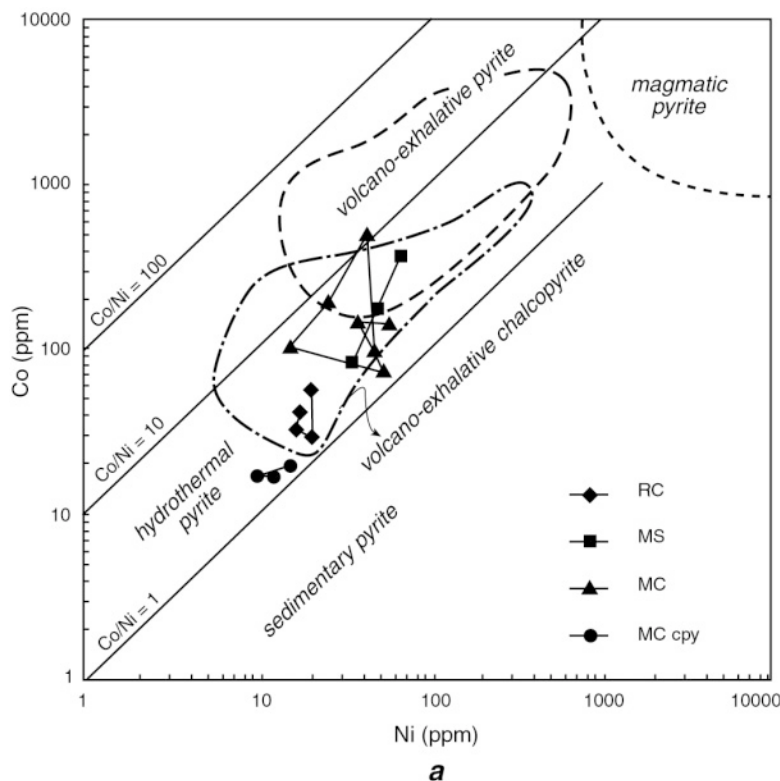


FIG. 14. Plot of the Co and Ni contents in MC chalcopyrite and mixtures of pyrite and chalcopyrite from RC, MS and MC ores of the Corvo orebody. Fields of pyrite and chalcopyrite of various origins, after Brill (1989) and Bajwah *et al.* (1987), are shown for comparison.

characterized by higher Fe, W, Ti and In contents than other VMS cassiterite. The high W contents suggest the deposition of cassiterite by high-temperature W-bearing fluids or a contribution of metals from a magmatic source (Seifert *et al.* 1997, Hennigh & Hutchinson 1997). This latter possibility is in accordance with the inferred origin of the sulfides. As Ti is mobile only under very strongly reducing conditions, the high concentrations in cassiterite from Corvo suggest that the Sn-transporting fluids were highly reduced (Seifert *et al.* 1997). Moreover, In is an element generally affiliated with high-temperature Cu mineralization and a probable magmatic source for metals (Schwarz-Schampera & Herzig 1997). These overall features suggest that cassiterite from Corvo was deposited by high-temperature (at least 350°C) fluids with a dominant magmatic signature.

As a whole, geochemical evidence indicates the origin of sulfides and cassiterite to be from magmatic fluids. Moreover, because textural evidence indicates the early crystallization of cassiterite, partially contempo-

raneously with arsenopyrite, we contend that cassiterite and the sulfides were deposited from the same magmatic fluids. Actually, this latter feature is not unusual, as it has been observed in other cassiterite-sulfide deposits (Heinrich & Eadington 1986). However, the question of the source of tin remains open. In this regard, Sn may have been derived from a granitic pluton that is probably present at depth (Gaspar 2002).

Genetic relationships between rubané and massive ores

The mineralogical and geochemical data presented in this paper support the hypothesis based on geological evidence (Relvas *et al.* 1997, Silva *et al.* 1997) indicating that the *rubané* ore, despite its stratigraphic position on top of the Corvo massive orebody, represents part of the stockwork of massive ore. In favor of the above hypothesis are the following lines of evidence.

i) The presence of tennantite (As-rich member) with very low Ag in *rubané* ore and of Ag-bearing tetrahe-

drite (Sb-rich member) in massive ore is consistent with the fact that stockwork ore in the IPB deposits is generally depleted in Sb and Ag compared to the massive ore (Marcoux *et al.* 1996).

ii) The As, Co and Sb contents of arsenopyrite from *rubané* ore are lower than those in arsenopyrite from massive ore. In fact, in most IPB deposits, arsenopyrite from the stockwork contains lower As, Co and Sb than arsenopyrite from the massive ore (Marcoux *et al.* 1996).

iii) The In contents of sphalerite, chalcopyrite and tennantite from *rubané* ore are lower than those in sphalerite, chalcopyrite and tetrahedrite from massive ore. This is consistent with the fact that In contents in sphalerite and chalcopyrite increase with decreasing depth of deposition, *i.e.*, with evolution of the mineralizing process (Osipova *et al.* 1970). Moreover, the In contents of IPB deposits are usually higher in massive ore than in the stockwork (Marcoux *et al.* 1996).

iv) The Se content of chalcopyrite from *rubané* ore is higher than chalcopyrite from the massive ore. In fact, stockwork chalcopyrite is usually enriched in Se in comparison with the analogous sulfide from upper massive ore in Australian VMS deposits (Huston *et al.* 1995).

v) The Mn content of pyrite–chalcopyrite mixtures from RC ore is lower than that detected in the same minerals from massive ores. This fact is consistent with a general concentration of Mn in late fluids, thus supporting the hypothesis of the early formation of RC ore, as part of the stockwork, with respect to massive ores, in a model of all Corvo fluids belonging to the same line of descent.

CONCLUSIONS

An ore-microscopy study of selected samples permits us to distinguish three main stages for Corvo mineralization. Stage I was characterized by deposition of sphalerite I and pyrite I, the latter showing typically atoll, colloform and radial structures. In contrast, during Stage II, which was the main stage of mineralization, there was deposition of cassiterite, arsenopyrite I and pyrite II, followed by sphalerite II, k esterite, tetrahedrite–tennantite, arsenopyrite II and galena, and, lastly, abundant chalcopyrite I, which enclosed and replaced early minerals, in some cases infilling fractures. Finally, Stage III was characterized by deposition of stannite, chalcopyrite II and carbonates, in veinlets cross-cutting the mineralization.

The application of EPMA and, especially, microPIXE analytical techniques allowed us to determine the trace-element distribution among the minerals from the various types of ore. In particular, the high Sn and In contents, compared with the analogous values in the ores from other VMS deposits (Marcoux *et al.* 1996), the Se/S and Co/Ni values as well as the Mn contents of pyrite, indicate a magmatic signature for the mineralizing fluids. This inference, along with the textural

relationships showing early crystallization of cassiterite, partially contemporaneous with arsenopyrite, indicates that the same magmatic fluids deposited cassiterite and sulfides. The fluids were highly reduced, because tin is transported in hydrothermal solutions mostly as Sn²⁺ chloro complexes. However, the deposition of SnO₂ took place under more oxidized conditions. Moreover, the high Cu grades of the Corvo deposit may indicate that the hydrothermal system was located close to the volcanic–magmatic center, in the area characterized by circulation of high-T fluids of deep emanation (Large 1992).

The main stage of mineralization was characterized by a relatively high temperature of formation (about 350°C) for both the *rubané* and the massive ores, as calculated by the application of the geothermometers based on the compositions of arsenopyrite and the sphalerite–k esterite pair, as well as the ^{IV}Al content in chlorite. Considering both the calculated temperatures and the observed assemblages of minerals, we estimate that log *a*(S₂) and log *a*(O₂) ranged between –7 to –12, and –26 to –29, respectively, whereas pH ranged between 3.4 and 4.9, except during deposition of carbonates in Stage III.

Finally, our ore-microscopy observations and geochemical data corroborate the hypothesis that *rubané* ore, located on the top of the massive ore, was originally a part of the stockwork of the VMS deposit, later displaced to its present-day position, presumably by Late Hercynian tectonics.

ACKNOWLEDGEMENTS

The authors thank the SOMINCOR (Sociedade Mineira de Neves Corvo, SA) for authorizing sampling in the early '90s, the CNR and JNICT for providing the funds for the sampling campaign in the context of the scientific co-operation agreement between Italy and Portugal, the CNR, "Centro di Studio per gli Equilibri Sperimentali in Minerali e Rocce", and the MURST for financial support (60%). Thanks are also given to Gilles Laflamme for EPMA analyses done at CANMET. We are also grateful for reviews by J.B. Maynard, an anonymous referee and Associate Editor E.M. Ripley, as well as the suggestions of Editor R.F. Martin.

REFERENCES

- ALBOUY, L., CONDE, L. N., FOGlierINI, F., LECA, X., MORIKIS, A., CALLIER, L., CARVALHO, P. & SONGY, J.G. (1981): Le gisement de sulfures massifs polym etalliques de Neves–Corvo (Baixo Alentejo, Sud Portugal). *Chron. Rech. Mini re* **49**(460), 5–27.
- BAJWAH, Z.U., SECCOMBE, P.K. & OFFLER, R. (1987): Trace element distribution; Co:Ni ratios and genesis of the Big Cadia iron–copper deposit, New South Wales, Australia. *Mineral. Deposita* **22**, 292–300.

- BARBANSON, L., SAULAS, D. & TOURAY, J.-C. (1985): Les blends mercurifères de la région de Cabezon de la Sal (Santander, Espagne). *Bull. Minéral.* **108**, 483-486.
- BARTON, P.B., JR. & TOULMIN, P., III (1966): Phase relations involving sphalerite in the Fe–Zn–S system. *Econ. Geol.* **61**, 815-849.
- BONIFAZI, G. & SERRANTI, S. (1996): Correlazione tra variazione di composizione chimica e colore in cristalli di cassiterite zonati mediante tecniche di analisi digitale delle immagini. *Atti V Workshop GIAST (San Sepolcro, Arezzo)*. De Frede, ed., Napoli, Italy (53-62).
- BORTNIKOV, N.S., GENKIN, A.D. & TRONEVA, N.V. (1993): Tennantite decomposition: evidence from the Kedabek copper deposit, Azerbaijan. *Mineral. Petrol.* **47**, 171-181.
- BRILL, B.A. (1989): Trace-element contents and partitioning of elements in ore minerals from the CSA Cu–Pb–Zn deposit, Australia. *Can. Mineral.* **27**, 263-274.
- CABRI, L.J. & CAMPBELL, J.L. (1998): The proton microprobe in ore mineralogy (micro-PIXE technique). In *Modern Approaches to Ore and Environmental Mineralogy* (L.J. Cabri & D.J. Vaughan, eds.). *Mineral. Assoc. Can., Short Course Vol. 27*, 181-198.
- _____, _____, LAFLAMME, J.H.G., LEIGH, R.G., MAXWELL, J.A. & SCOTT, J.D. (1985): Proton-microprobe analysis of trace-elements in sulfides from massive-sulfide deposits. *Can. Mineral.* **23**, 133-148.
- _____, GASPAR, O.C., LASTRA, R. & MCMAHON, G. (1998): Distribution of gold in tin-rich samples from the Corvo orebody, Portugal. *Can. Mineral.* **36**, 1347-1360.
- CAMPBELL, J.L., MAXWELL, J.A., TEESDALE, W.J., WANG, J.-X. & CABRI, L.J. (1990): Micro-PIXE as a complement to electron probe microanalysis in mineralogy. *Nuclear Instrum. Methods Phys. Res.* **B44**, 347-356.
- CARVALHO, D. (1979): Geologia, metalogenia e metodologia da investigação de sulfuretos polimetálicos do Sul de Portugal. *Comun. Serv. Geol. Portugal* **65**, 169-191.
- _____, BARRIGA, F.J.A.S. & MUNHÁ, J. (1997): Bimodal siliciclastic systems; the case of the Iberian Pyrite Belt. In *Volcanic-Associated Massive Sulfide Deposits: Processes and Examples in Modern and Ancient Settings* (C.T. Barrie & M.D. Hannington, eds.). *Rev. Econ. Geol.* **8**, 375-408.
- _____, NABAIS-CONDE, L.E., HERNANDEZ-ENRILE, J., OLIVEIRA, V., SCHERMERHORN, L.J.G.S. GARCIA-PALOMERO, F., LOPERA-CABALLERO, E., MADEL, J. & MARTIN, E. (1976): Livro-Guia das Excursões Geológicas na Faixa Piritosa Iberica. *Comun. Serv. Geol. Portugal* **60**, 271-315.
- CATHELINÉAU, M. & NIEVA, D. (1985): A chlorite solid solution geothermometer. The Los Azufres (Mexico) geothermal system. *Contrib. Mineral. Petrol.* **91**, 235-244.
- EUGSTER, H.P. (1986): Minerals in hot water. *Am. Mineral.* **71**, 655-673.
- FLEISCHER, M. (1955): Minor elements in some sulfide minerals. *Econ. Geol., Fiftieth Anniv. Vol., II*, 970-1024.
- GARCIA DE MIGUEL, J.M. (1990): Mineralogía, paragénesis y sucesión de los sulfuros masivos de la Faja Piritica en el suroeste de la Península Ibérica. *Boletín Geológico y Minero* **101**, 73-105.
- GASPAR, O.C. (1991): Paragenesis of the Neves–Corvo volcanogenic massive sulphides. *Comun. Serv. Geol. Portugal*, **77**, 27-52.
- _____. (1997): Ore microscopy applied to the beneficiation of volcanogenic massive sulfides. *Explor. Mining Geol.* **6**, 335-348.
- _____. (2002): Mineralogy and sulfide mineral chemistry of the Neves–Corvo ores, Portugal: insight into their genesis. *Can. Mineral.* **40**, 611-636.
- _____. & PINTO, A. (1993): Neves–Corvo, a Kuroko type deposit in the Iberian Pyrite Belt. *Proc. 29th Int. Geol. Congress (Kyoto), J. Res. Geol., Spec. Issue 17*, 249-262.
- GIULIANI, G. (1987): La cassitérite zonée du gisement de Sokhret Allal (granite des Zaër; Maroc central): composition chimique et phases fluides associées. *Mineral. Deposita* **22**, 253-261.
- HEINRICH, C.A. & EADINGTON, P.J. (1986): Thermodynamic predictions of hydrothermal chemistry of arsenic, and their significance for the paragenetic sequence of some cassiterite – arsenopyrite – base metal sulfide deposits. *Econ. Geol.* **81**, 511-529.
- HENNIGH, Q.T. & HUTCHINSON, R.W. (1997): Geology of the tin-rich ores of the Corvo orebody, Neves–Corvo deposit, Portugal. In *SEG Neves Corvo Field Conference 1997* (F.J.A.S. Barriga, ed.). Lisbon, Portugal (96).
- HUSTON, D.L., SIE, S.H., SUTER, G.F., COOKE, D.R. & BOTH, R.A. (1995): Trace elements in sulfide minerals from eastern Australian volcanic-hosted massive sulfide deposits. I. Proton microprobe analyses of pyrite, chalcopyrite, and sphalerite. II. Selenium levels in pyrite: comparison with $\delta^{34}\text{S}$ values and implications for the source of sulfur in volcanogenic hydrothermal systems. *Econ. Geol.* **90**, 1167-1196.
- IZORET, L., MARNIER, G. & DUSAUSOY, Y. (1985): Caractérisation cristallochimique de la cassitérite des gisements d'étain et de tungstène de Galice, Espagne. *Can. Mineral.* **23**, 221-231.
- JOHAN, Z. (1988): Indium and germanium in the structure of sphalerite: an example of coupled substitution with copper. *Mineral. Petrol.* **39**, 211-229.
- KOJIMA, S. & SUGAKI, A. (1985): Phase relations in the Cu–Fe–Zn–S system between 500° and 300°C under hydrothermal conditions. *Econ. Geol.* **80**, 158-171.
- KRETSCHMAR, V. & SCOTT, S.D. (1976): Phase relations involving arsenopyrite in the system Fe–As–S and their application. *Can. Mineral.* **14**, 364-386.

- LARGE, R.R. (1992): Australian volcanic-hosted massive sulfide deposits: features, styles, and genetic models. *Econ. Geol.* **87**, 471-510.
- LECA, X., RIBEIRO, A., TOMAS OLIVEIRA, J., BRANDAO SILVA, J., ALBOUY, L., CARVALHO, P. & MERINO, H. (1983): Cadre géologique des minéralisations de Neves-Corvo (Baixo-Alentejo, Portugal): lithostratigraphie, paléogéographie et tectonique. *Mém. BRGM* **121**, 80.
- LEGENDRE, O. (1994): Indium in base-metal sulfides from various occurrences: new data. *Int. Mineral. Assoc., 16th Gen. Meeting (Pisa)*, 237 (abstr.).
- LEISTEL, J.M., MARCOUX, E., THIÉBLEMONT, D., QUESADA, C., SÁNCHEZ, A., ALMODOVAR, G.R., PASCUAL, E. & SAEZ, R. (1998): The volcanic-hosted massive sulphide deposits of the Iberian Pyrite Belt. Review and preface to the Thematic Issue. *Mineral. Deposita* **33**, 2-30.
- LEITCH, C.H.B. (1981): Mineralogy and textures of the Lahanos and Kizilkaya massive sulfide deposits, northeastern Turkey, and similarity to Kuroko ores. *Mineral. Deposita* **16**, 241-257.
- MARCOUX, E., MOËLO, Y. & LEISTEL, J.M. (1996): Bismuth and cobalt minerals as indicators of stringer zones to massive sulfide deposits, Iberian Pyrite Belt. *Mineral. Deposita* **31**, 1-26.
- MAXWELL, J.A., CAMPBELL, J.L. & TEESDALE, W.J. (1989): The Guelph PIXE software package. *Nucl. Instr. Methods Phys. Res.* **B43**, 218-230.
- _____, TEESDALE, W.J. & CAMPBELL, J.L. (1995): The Guelph PIXE software package II. *Nucl. Instr. Methods Phys. Res.* **B95**, 407-421.
- MÖLLER, P., DULSKI, P., SZACKI, W., MALOW, G. & RIEDEL, E. (1988): Substitution of tin in cassiterite by tantalum, niobium, tungsten, iron and manganese. *Geochim. Cosmochim. Acta* **52**, 1497-1503.
- MURCIEGO, A., GARCIA SANCHEZ, A., DUSAUSOY, Y., MARTIN POZAS, J.M. & RUCK, R. (1997): Geochemistry and EPR of cassiterites from the Iberian Hercynian Massif. *Mineral. Mag.* **61**, 357-365.
- NAKAMURA, Y. & SHIMA, H. (1982): Fe and Zn partitioning between sphalerite and stannite. *Soc. Mining Geol. Japan – Mineral. Soc. Japan*, A-8.
- NEIVA, A.M.R. (1996): Geochemistry of cassiterite and its inclusions and exsolution products from tin and tungsten deposits in Portugal. *Can. Mineral.* **34**, 745-768.
- OLIVEIRA, J.T., PACHECO, N., CARVALHO, P. & FERREIRA, A. (1997): The Neves Corvo mine and the Paleozoic geology of southwest Portugal. In *Geology and VMS Deposits of the Iberian Pyrite Belt. SEG Neves Corvo Field Conference 1997* (F.J.A.S. Barriga & D. Carvalho, eds.). *Soc. Econ. Geol., Guidebook Ser.* **27**, 21-71.
- OSIPOVA, G.A., RADKEVICH, E.A. & KOKORIN, A.M. (1970): Geochemical criteria of the depths of mineralization for some tin and complex ore deposits in the Far East of the U.S.S.R. *Endogenie Rudnykh Mestorozhdenii*, 136-145.
- PATTERSON, D.J., OHMOTO, H. & SOLOMON, M. (1981): Geologic setting and genesis of cassiterite-sulfide mineralization at Renison Bell, western Tasmania. *Econ. Geol.* **76**, 393-438.
- PATRICK, R.A.D. & DORLING, M. (1991): The substitution of indium and copper in natural sphalerite: a study using electron microscopy. In *Source, Transport and Deposition of Metals* (M. Pagel & J.L. Leroy, eds.). A.A. Balkema, Rotterdam, The Netherlands (223-226).
- PETRUK, W. (1973): Tin sulphides from the deposit of Brunswick Tin Mines Limited. *Can. Mineral.* **12**, 46-54.
- PINTO, A., FERREIRA, A., BOWLES, J.F.W. & GASPAS, O.C. (1997): Mineralogical and textural characterization of the Neves-Corvo ores. Metallogenetic implications. In *SEG Field Conference 1997* (F.J.A.S. Barriga, ed.), Lisbon, Portugal (90).
- REAL, F. & CARVALHO, P. (1997): GEOMMINCOR: successful scientific – industrial interaction in the geological investigation of the Neves Corvo mineral deposits. In *SEG Field Conference 1997* (F.J.A.S. Barriga, ed.), Lisbon, Portugal (84).
- RELVAS, J.M.R.S., BARRIGA, F.J.A.S., FERREIRA, A., NOIVA, P.C. & FONSECA P. (1997): Copper enrichment by ductile remobilization at Neves Corvo, Portugal. In *SEG Field Conference 1997* (F.J.A.S. Barriga, ed.), Lisbon, Portugal (112).
- REMOND, G., CESBRON, F., TRAXEL, K., CAMPBELL, J.L. & CABRI, L.J. (1987): Electron microprobe analysis and proton induced X-ray spectrometry applied to trace elements in sulfides: problems and prospects. *Scanning Microsc.* **1**, 1017-1037.
- ROUTHIER, P., AYE, F., BOYER, C., LÉCOLLE, M., PICOT, P. & ROGER, G. (1980): La ceinture sud-ibérique à amas sulfurés dans sa partie espagnole médiane. Tableau géologique et métallogénique. Synthèse sur le type d'amas sulfurés volcano-sédimentaires. *Mém. BRGM* **94**.
- SCHWARZ-SCHAMPERA, U. & HERZIG, P.M. (1997): Mineralogy and geochemistry of indium in massive sulfides from the Lau Basin (southwest Pacific). In *SEG Field Conference 1997* (F.J.A.S. Barriga, ed.), Lisbon, Portugal (32).
- SCOTT, S.D. (1983): Chemical behaviour of sphalerite and arsenopyrite in hydrothermal and metamorphic environments. *Mineral. Mag.* **47**, 427-435.
- _____, & BARNES, H.L. (1971): Sphalerite geothermometry and geobarometry. *Econ. Geol.* **66**, 653-669.
- SEAL, R.R., II, ESSENE, E.J. & KELLY, W.C. (1990): Tetrahedrite and tennantite: evaluation of thermodynamic data and phase equilibria. *Can. Mineral.* **28**, 725-738.

- SEIFERT, T., SCHWARZ-SCHAMPERA, U., HERZIG, P.M., HUTCHINSON, R.W., HENNIGH, Q. & WAGNER, R. (1997): Trace element characteristics of cassiterite in granite-related tin and tin-bearing VMS deposits. *In* SEG Field Conference 1997 (F.J.A.S. Barriga, ed.), Lisbon, Portugal (113).
- SERRANTI, S. (1998): *Le mineralizzazioni "rubané" e massiva del giacimento a Cu-Sn di Corvo (Neves-Corvo, Portogallo): studio metallografico e geochimico, implicazioni genetiche e applicazione di tecniche di analisi d'immagine*. Ph.D. thesis, Dipartimento di Scienze della Terra, Università di Roma "La Sapienza", Rome, Italy.
- SHIMIZU, M., KATO, A. & SHIOZAWA, T. (1986): Sakuraiite: chemical composition and extent of (Zn,Fe)In-for-CuSn substitution. *Can. Mineral.* **24**, 405-409.
- _____ & SHIKAZONO, N. (1985): Fe and Zn partitioning between coexisting stannite and sphalerite: a possible indicator of temperature and sulfur fugacity. *Mineral. Deposita* **20**, 314-320.
- SILVA, J.B., RIBEIRO, A., FONSECA., OLIVEIRA, J.T., PEREIRA, Z., FERNANDES, J.P., BARRIGA, F.J.A.S., RELVAS, J.M.R.S., CARVALHO, P., FERREIRA, A., BELIZ, A., CAETANO, P., PACHECO, N. & ALBERNAZ, J. (1997): Tectonostratigraphic overview of Neves-Corvo mine in the context of the Variscan orogeny. *In* SEG Field Conference 1997 (F.J.A.S. Barriga, ed.), Lisbon, Portugal (88).
- STRAUSS, G.K., MADEL, J.E & FERNANDEZ-ALONSO, F. (1977): Exploration practice for stratabound volcanogenic sulfide deposits in the Spanish-Portuguese Pyrite Belt: geology, geophysics and geochemistry. *In* Time and Stratabound Ore Deposits (D.D. Klemm & H.J. Schneider, eds.). Springer Verlag, Berlin, Germany (55-93).
- TAYLOR, J.R. & WALL, V.J. (1993): Cassiterite solubility, tin speciation, and transport in a magmatic aqueous phase. *Econ. Geol.* **88**, 437-460.
- UDUBAŞA, G. (1984): Iron sulfides in sedimentary rocks, some occurrences in Romania. *In* Syngeneses and Epigenesis in the Formation of Mineral Deposits (A. Wanschkuhn, C. Kluth & R.A. Zimmermann, eds.). Springer Verlag, Berlin, Germany (28-35).
- VELASCO, F., SÁNCHEZ-ESPAÑA, J., BOYCE, A.J., FALLICK, A.E., SÁEZ, R. & ALMODÓVAR, G.R. (1998): A new sulfur isotopic study of some Iberian Pyrite Belt deposits: evidence of a textural control on sulfur isotope composition. *Mineral. Deposita* **34**, 4-18.
- XUEXIN, SONG (1984): Minor elements and ore genesis of the Fankou lead-zinc deposit, China. *Mineral. Deposita* **19**, 95-104.

Received November 3, 2001, revised manuscript accepted April 24, 2002.